Cell

Phase 1/2a clinical trial of hESC-derived dopamine progenitors in Parkinson's disease

Graphical abstract

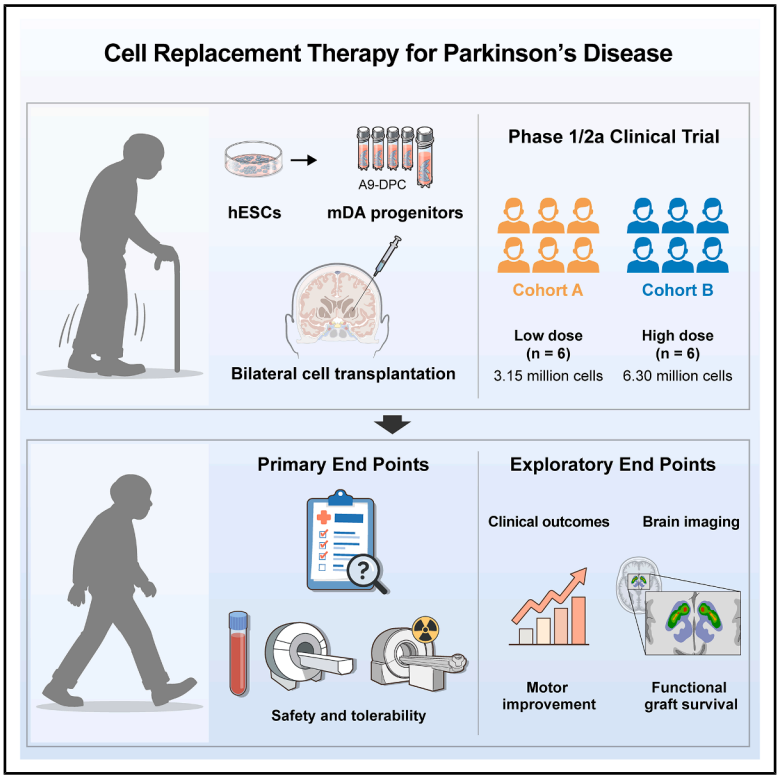

Highlights

- We generated high-purity dopaminergic progenitors (A9-DPC) from hESCs
- Bilateral transplantation of A9-DPC in putamen was safe in patients with PD
- A9-DPC transplantation improved motor symptoms, with greater efficacy at high doses
- Dopamine transporter binding on PET increased, especially in the high-dose group

Authors

Jin Woo Chang, Han Kyu Na, Kyung Won Chang, ..., Myung Soo Cho, Phil Hyu Lee, Dong-Wook Kim

Correspondence

phlee@yuhs.ac (P.H.L.), dwkim2@yuhs.ac (D.-W.K.)

In brief

High-purity dopaminergic progenitors were generated from human embryonic stem cells, and their safety and exploratory efficacy were evaluated in a single-center, open-label, dose-escalation phase 1/2a trial for patients with Parkinson's disease.

Chang et al., 2025, Cell *188*, 7036–7048
December 11, 2025
https://doi.org/10.1016/j.cell.2025.09.010

CellPress

CellPress
OPEN ACCESS

Cell

Article

Phase 1/2a clinical trial of hESC-derived dopamine progenitors in Parkinson's disease

Jin Woo Chang,[1,11] Han Kyu Na,[2,11] Kyung Won Chang,[3,11] Chan Wook Park,[2,4,11] Do-Hun Kim,[4,5] Sanghyun Park,[4] Chul-Yong Park,[4,5] Jang Hyeon Eom,[5] Seung Taek Nam,[5] Ki-Sang Jo,[5] Mi-Young Jo,[5] Sung Kyoung Choi,[5] Hye-Jin Hur,[5] Sarang Kim,[5] Minseok Kim,[6] Dae-Sung Kim,[7] Dong-Youn Hwang,[8] Myoung Soo Kim,[9] Inkyung Jung,[6] Jongwan Kim,[5] Myung Soo Cho,[5] Phil Hyu Lee,[2,*] and Dong-Wook Kim[4,5,10,12,*]

[1]Department of Neurosurgery, Korea University Anam Hospital, Seoul 02841, Republic of Korea
[2]Department of Neurology, Yonsei University College of Medicine, Seoul 03722, Republic of Korea
[3]Department of Neurosurgery, Samsung Medical Center, Sungkyunkwan University School of Medicine, Seoul 06351, Republic of Korea
[4]Department of Physiology, Yonsei University College of Medicine, Seoul 03722, Republic of Korea
[5]S. Biomedics Co., Ltd., Seoul 04797, Republic of Korea
[6]Division of Biostatistics, Department of Biomedical Systems Informatics, Yonsei University College of Medicine, Seoul 03722, Republic of Korea
[7]Department of Biotechnology, College of Life Sciences and Biotechnology, Korea University, Seoul 02841, Republic of Korea
[8]Department of Biomedical Science, CHA University, Seongnam, Gyeonggi-do 13488, Republic of Korea
[9]Department of Surgery, Yonsei University College of Medicine, Seoul 03722, Republic of Korea
[10]Brain Korea 21 PLUS Program for Medical Science, Yonsei University College of Medicine, Seoul 03722, Republic of Korea
[11]These authors contributed equally
[12]Lead contact
*Correspondence: phlee@yuhs.ac (P.H.L.), dwkim2@yuhs.ac (D.-W.K.)
https://doi.org/10.1016/j.cell.2025.09.010

SUMMARY

Parkinson's disease (PD) has long been considered an appropriate candidate for cell replacement therapy. We generated high-purity dopaminergic progenitors (A9-DPCs) from human embryonic stem cells and evaluated their safety and exploratory efficacy in a single-center, open-label, dose-escalation phase 1/2a trial (NCT05887466) for PD patients. Twelve patients with moderate-to-severe PD received bilateral putamen transplantation of low-dose (3.15 million cells; $n = 6$) or high-dose (6.30 million cells; $n = 6$) A9-DPC with immunosuppression. No dose-limiting toxicities or graft-related adverse events were observed. At 12 months, off-medication Movement Disorder Society Unified Parkinson's Disease Rating Scale (MDS-UPDRS) part III scores and Hoehn and Yahr stage improved, with greater motor improvements in the high-dose group. Dopamine transporter positron emission tomography (PET) imaging showed increased posterior putamen uptake with greater uptake in the high-dose group after transplantation, supporting graft survival. These findings indicate that bilateral transplantation of A9-DPC is safe and may improve parkinsonian motor symptoms in patients with PD.

INTRODUCTION

Parkinson's disease (PD) is a progressive neurodegenerative disorder characterized by the selective loss of dopaminergic (DA) neurons in the substantia nigra pars compacta, leading to striatal dopamine depletion and the emergence of motor symptoms.[1] Although pharmacological treatments and deep brain stimulation (DBS) provide symptomatic relief, they cannot prevent the progressive loss of DA neurons and often result in motor complications.[2] Given its well-defined pathological hallmark, the loss of a specific DA neuronal population, PD has long been considered an ideal candidate for cell-based regenerative therapy.[3] While DA cell transplantation is currently considered a symptomatic treatment for partial dopamine compensation, it differs from conventional therapies by replenishing lost DA neurons[4] and enabling sustained, spatially targeted dopamine release in physiologically relevant striatal regions. Consequently, efforts have been directed toward targeted restoration of dopamine function through the transplantation of DA cells in the putamen.[5,6]

Early attempts at cell therapy in PD involved the transplantation of fetal ventral mesencephalic tissue containing DA progenitors, demonstrating promising initial results in open-label studies.[7–9] However, subsequent randomized trials yielded inconsistent outcomes, and the application of fetal tissue transplantation was limited by ethical concerns, restricted tissue availability, and cellular heterogeneity.[10,11] The development of human pluripotent stem cells (hPSCs), including human embryonic stem cells (hESCs) and induced PSCs (iPSCs), has provided a scalable source for generating DA progenitors.[12] Advances in

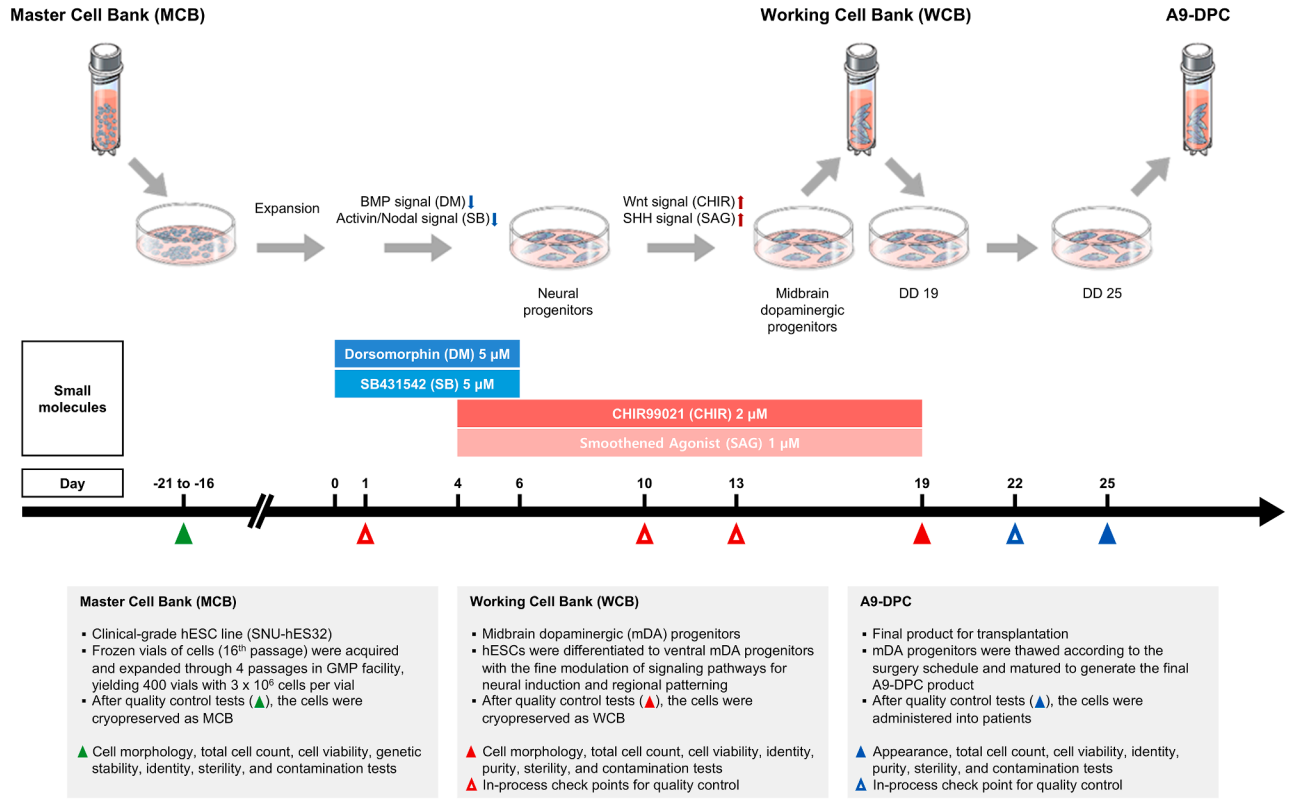

Figure 1. A schematic diagram of A9-DPC preparation

Clinical-grade hESCs (SNU-hES32) were differentiated into mDA progenitors using a good manufacturing practice (GMP)-compliant culture system. Thawed vials from the master cell bank (MCB) were plated on dishes and exposed to 5 μM dorsomorphin (DM), an inhibitor of BMP signaling, and 5 μM SB431542 (SB), an inhibitor of activin/nodal signaling, for 1 day to initiate dual SMAD inhibition. Neural induction was then promoted by culturing the cells as aggregates in suspension under continued dual SMAD inhibition for 5 days. The aggregates were then replated and cultured adherently. After 4 days of attachment, rosette-like columnar structures emerged and were manually isolated. Cells were differentiated over a 15-day period (from differentiation day [DD] 4 to DD 19) in the presence of 1 μM smoothened agonist (SAG) and 2 μM CHIR99021 (CHIR), which activate Sonic Hedgehog (SHH) and Wnt signaling pathways, respectively. On DD 19, cells were cryopreserved to establish a WCB. For clinical use, WCB vials were thawed and further cultured until DD 25 to generate the final A9-DPC product for transplantation. Only batches that passed all predefined QC criteria were used for patient transplantation. A break in the axis indicates a discontinuity in scale. See also Tables S1 and S2.

differentiation protocols have enabled the production of high-purity DA progenitors on a large scale that exhibit graft survival and behavior recovery in preclinical models.[13]

The successful clinical translation of hPSC-derived DA cell transplantation necessitates the stringent evaluation of both safety and efficacy. A key safety concern is the potential for tumorigenicity and uncontrolled proliferation of transplanted DA progenitors. Additionally, for optimal therapeutic benefit, transplanted DA progenitors must exhibit robust survival, maturation into functional DA neurons, and appropriate integration into host neural circuits. These factors have been extensively evaluated in preclinical studies, which have demonstrated encouraging safety profiles and functional recovery in PD models, paving the way for further clinical translation.[14–18]

Based on our previous preclinical study,[16] the Ministry of Food and Drug Safety (MFDS) in Korea approved the transplantation of hESC-derived DA progenitors (A9-DPCs, also called TED-A9) in patients with PD. These progenitors were differentiated using a fully defined, three-dimensional (3D)-based protocol that exclusively utilizes small molecules, enabling the large-scale generation of ventral midbrain DA (mDA) progenitors with high purity. Unlike cryopreserved, off-the-shelf products, we transplanted freshly cultured cells, which demonstrated superior functional improvement and DA cell survival in a parkinsonian rat model in a dose-dependent manner.[16] Based on these rigorous preclinical dose-response assessments, we determined the cell numbers for the low-dose (n = 6) and high-dose groups (n = 6) for the clinical trial. Herein, we report the 1-year interim results of a phase 1/2a trial evaluating the safety and exploratory efficacy of transplantation of A9-DPC in patients with PD.

RESULTS

A9-DPC manufacturing

A9-DPC was manufactured from a clinical-grade hESC line (SNU-hES32) under good manufacturing practice (GMP)-compliant conditions using a standardized small-molecule differentiation protocol as described in detail in our previous preclinical study[16] and summarized in Figure 1. Differentiated

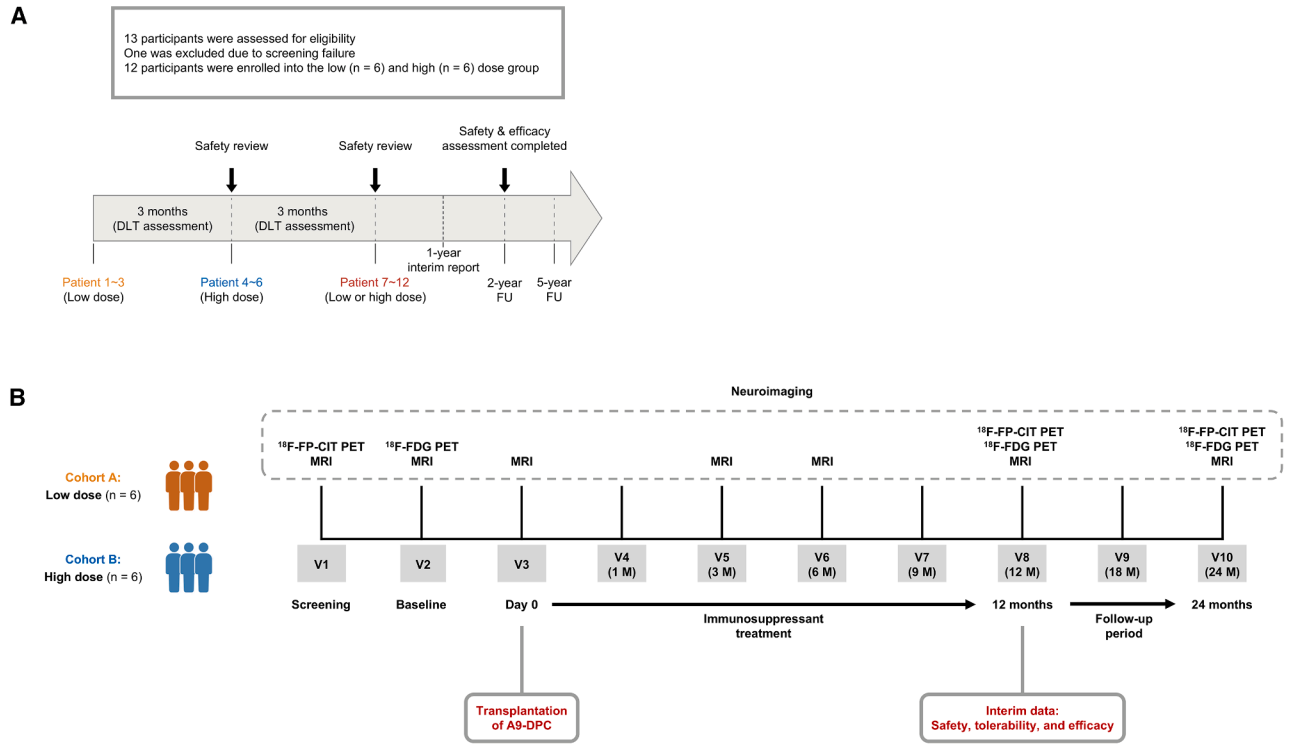

Figure 2. Trial design

(A) Overview of patient enrollment and study plan. Thirteen patients were assessed for eligibility, and twelve participants were finally enrolled in either the low-dose (3.15 million cells) or high-dose (6.30 million cells) group. Dose escalation followed a standard 3 + 3 rule-based design. The SRC evaluated 3-month safety data (DLT) after each cohort, permitting dose escalation and subsequent cohort expansion. Participants undergo a 2-year follow-up (FU) after transplantation, with an interim report generated at 12 months based on predefined clinical and imaging assessments. An additional long-term FU study is planned to monitor safety for up to 5 years.

(B) Clinical FU schedule for each patient. Each patient was assessed at visit (V) 1, and baseline evaluations were conducted at V2 for enrolled participants. Scheduled clinical and imaging assessments were performed over 12 months for interim analysis. Immunosuppressants were administered for up to 12 months. V1, screening; V2, baseline; V3, transplantation of A9-DPC; V4, 1 month; V5, 3 months; V6, 6 months; V7, 9 months; V8, 12 months; V9, 18 months; V10, 24 months after transplantation.

See also Tables S6 and S7.

mDA progenitors were cryopreserved on differentiation day (DD) 19 to establish a working cell bank (WCB), then thawed according to the surgery schedule and further cultured to DD 25 prior to transplantation. Among 13 clinical batches from WCB, 12 passed predefined quality control (QC) criteria (Tables S1 and S2). One batch was excluded owing to mycoplasma contamination, and the corresponding patient's surgery was rescheduled with a newly prepared batch. Final products (A9-DPC) were vialed and refrigerated (2°C–8°C) for shipment and administered within 36 h post-release.

Participants and trial procedures

Thirteen patients were assessed for eligibility, and one was excluded due to screening failure. Twelve participants were enrolled and assigned to a low-dose (3.15 million cells, $n = 6$) or high-dose (6.30 million cells, $n = 6$) group. Dose escalation followed a standard 3 + 3 rule-based design (Figure 2A), in which an initial cohort of three patients underwent intracerebral transplantation of low-dose A9-DPC. No dose-limiting toxicity (DLT), defined as a grade 3 or higher adverse event (AE) related to treatment according to the National Cancer Institute Common Terminology Criteria for Adverse Events (NCI CTCAE, version 5.0), was reported among the first three patients in the low-dose group during the initial 3-month period. After review of the safety data, the Safety Review Committee (SRC) approved the enrollment of three additional patients in the high-dose group. Following another 3-month observation, with no DLT reported, the SRC conducted a second evaluation and approved the expansion of the enrollment of three additional patients in each dose group. Thus, the transplantation was completed with a total of 12 patients enrolled, and the patients were evaluated for safety and exploratory efficacy for the first 12 months (1-year interim report) (Table 1).

Scheduled clinical and imaging assessments, including brain magnetic resonance imaging (MRI), ^{18}F-N-(3-fluoropropyl)-2β-carbomethoxy-3β-(4-iodophenyl) nortropane (^{18}F-FP-CIT) positron emission tomography (PET), and ^{18}F-fluorodeoxyglucose (^{18}F-FDG) PET, were performed (Figure 2B). Immunosuppressants, including basiliximab, methylprednisolone/prednisolone, and tacrolimus, were administered for up to 12 months.

Table 1. List of primary and exploratory endpoints during the 12-month follow-up period

Primary	
Objectives	Endpoints (incidence of AEs)
Safety and tolerability of A9-DPC	treatment-emergent AEs
	AEs of special interest
	infectious disease
	complications related to surgical procedures
	formations of neoplasms or malignancies
	immune responses, including exacerbation or new onset of autoimmune diseases
	other delayed AEs related to the cell therapy
	death
Exploratory	
Objectives	Endpoints (change from baseline)
Efficacy and safety of A9-DPC based on clinical outcomes	MDS-UPDRS score: part III (on and off), part IV, total (on and off)
	H&Y stage (on and off)
	PDQ-39
	SE-ADL
	NMSS
	K-MMSE
	K-MoCA
	PD diary: off time
	LEDD
Efficacy and safety of A9-DPC based on imaging outcomes	brain MRI scan
	^{18}F-FDG PET scan: cerebral and striatal ^{18}F-FDG uptake
	^{18}F-FP-CIT PET scan: striatal ^{18}F-FP-CIT uptake

AEs, adverse events; MDS-UPDRS, Movement Disorder Society Unified Parkinson's Disease Rating Scale; PDQ, Parkinson's Disease Questionnaire; SE-ADL, Schwab and England Activities of Daily Living; NMSS, Non-Motor Symptoms Scale; K-MMSE, Korean versions of Mini-Mental State Examination; K-MoCA, Korean versions of Montreal Cognitive Assessment; PD, Parkinson's disease; LEDD, levodopa equivalent daily dose; MRI, magnetic resonance imaging; ^{18}F-FDG PET, ^{18}F-fluorodeoxyglucose positron emission tomography; ^{18}F-FP-CIT, ^{18}F-N-(3-fluoropropyl)-2β-carbomethoxy-3β-(4-iodophenyl) nortropane.

Baseline demographic and clinical characteristics were similar between the two groups and are summarized in Table 2. The mean age of the participants was 60.3 ± 5.0 years, and the mean duration since diagnosis was 10.5 ± 2.5 years. All participants' clinical presentations were consistent with moderate-to-severe PD.[19]

Primary outcomes: Safety and tolerability

Over the 12-month follow-up period, 32 AEs were recorded, and all AEs were assessed as definitely unrelated to the investigational product, A9-DPC (Table 3). Among these, one event was associated with the surgical procedure, and three events (two participants) were considered possibly related to immunosuppressants.

Regarding the surgery-related AE, one patient experienced an asymptomatic intracranial hemorrhage detected on postoperative computed tomography (CT) imaging at the right caudate. Among immunosuppressant-related AEs, one patient developed transient hyperkalemia 6 months postoperatively, which resolved promptly with medical treatment. Given the potential association with tacrolimus, a potassium-removing agent was administered prophylactically throughout the tacrolimus treatment period. Another patient was diagnosed with diabetes mellitus at 6 months and started oral antidiabetic medication. The same patient also developed thrombocytopenia at 3 months but remained asymptomatic, with normal white blood cell count, liver function tests, and abdominal imaging findings. Autoimmune tests and infectious evaluations were negative. Thus, no specific intervention was required, and the platelet count gradually improved with close monitoring. The thrombocytopenia prolonged hospitalization by 1 day and thus was reported as a serious AE (SAE), although no definitive cause was identified.

Overall, only one SAE occurred among the total of 12 patients during the 12-month follow-up. No evidence of tumor formation or abnormal graft overgrowth was observed. These findings collectively demonstrate the favorable safety and tolerability profile of A9-DPC transplantation during the 12-month observation period.

Exploratory clinical outcomes

The participants showed improvement in off-medication state (OFF) motor symptoms at 12 months compared with baseline, with a mean ± standard deviation (SD) change of

Table 2. Baseline demographic and clinical characteristics of the participants

	Low-dose (n = 6)[a]	High-dose (n = 6)[a]	Total (n = 12)[a]
Age (years)	60.0 ± 5.9	60.7 ± 4.6	60.3 ± 5.0
Male sex, no. (%)	5 (83.3)	4 (66.7)	9 (75.0)
Time since diagnosis (years)	9.2 ± 2.7	11.8 ± 1.6	10.5 ± 2.5
H&Y stage, off state[b]			
Stage 3, no. (%)	2 (33.3)	1 (16.7)	3 (25.0)
Stage 4, no. (%)	4 (66.7)	5 (83.3)	9 (75.0)
H&Y stage, on state[b]			
Stage 2, no. (%)	4 (66.7)	4 (66.7)	8 (66.7)
Stage 3, no. (%)	2 (33.3)	2 (33.3)	4 (33.3)
MDS-UPDRS score[c]			
Part I	19.7 ± 3.6	22.8 ± 7.0	21.3 ± 5.6
Part II	22.7 ± 5.1	26.2 ± 4.8	24.4 ± 5.1
Part III, on state	27.5 ± 3.0	25.5 ± 4.7	26.5 ± 3.9
Part III, off state	61.0 ± 9.1	57.7 ± 7.1	59.3 ± 8.0
Part IV	12.5 ± 2.6	14.3 ± 2.1	13.4 ± 2.4
NMSS, total score[d]	107.8 ± 18.6	113.8 ± 34.6	110.8 ± 26.7
PDQ-39 SI score[e]	31.6 ± 20.8	34.0 ± 12.7	32.8 ± 16.5
SE-ADL score[f]	0.5 ± 0.2	0.5 ± 0.1	0.5 ± 0.1

MDS-UPDRS, Movement Disorder Society Unified Parkinson's Disease Rating Scale; NMSS, Non-Motor Symptoms Scale; PDQ-39 SI, Parkinson's Disease Questionnaire-39 Summary Index; SE-ADL, Schwab and England Activities of Daily Living.
[a]Values are means ± standard deviation (SD). A total of 3.15 million (low-dose) and 6.30 million (high-dose) cells were administered.
[b]Stages range from 1 to 5, with higher stages indicating greater disease severity.
[c]Scores on MDS-UPDRS parts I and II range from 0 to 52, with higher scores indicating greater severity of impairment in non-motor (part I) or motor (part II) aspects of daily living. Scores on MDS-UPDRS part III range from 0 to 132, with higher scores indicating more severe impairment on a clinician-conducted motor examination. Scores on part IV range from 0 to 24, with higher scores indicating more severe motor complications.
[d]Scores on the NMSS range from 0 to 360, with higher scores indicating severe and frequent symptoms. The NMSS consists of 30 items across 9 domains, each rated by multiplying severity (0–3) and frequency (1–4), with domain and total scores calculated accordingly.
[e]Scores on the PDQ-39 SI range from 0 to 100, with higher scores indicating worse health status. The PDQ-39 includes 8 domains (each scored 0–4), with domain scores expressed as percentages and the PDQ-39 SI calculated as their average.
[f]Scores on the SE-ADL scale are normalized to the 0–1 range, with higher scores indicating a greater level of independence.

−14.1 ± 6.2 points (improvement) in the Movement Disorder Society Unified Parkinson's Disease Rating Scale (MDS-UPDRS) part III (OFF) scores (Table S3). The mean change in MDS-UPDRS part III (OFF) scores was −12.7 ± 8.2 points in the low-dose group and −15.5 ± 3.6 points in the high-dose group (Figure 3A). A significant group-by-time interaction was observed in the linear mixed-effects model, with a greater improvement over time in the high-dose group compared with the low-dose group (p = 0.019) (Figure 3B). Similarly, for the Hoehn and Yahr (H&Y) (OFF) stage, the mean ± SD change was −1.0 ± 0.6 points in the low-dose group and −1.7 ± 0.5 points (improvement) in the high-dose group at 12 months compared with baseline (Table S3; Figure 3C) with a more pronounced change across visits in the high-dose group compared with the low-dose group by the generalized linear mixed-effects model (p = 0.045).

In the on-medication state (ON), the participants showed no significant improvement of motor symptoms at 12 months compared with baseline, with a mean ± SD change of 0 ± 4.6 points in MDS-UPDRS part III (ON) scores (Table S3). The mean change in the MDS-UPDRS part III (ON) scores was −2.8 ± 4.5 points in the low-dose group and 2.8 ± 2.6 points in the high-dose group (Figure S1A). Likewise, for the H&Y (ON) stage, the mean ± SD change was −0.2 ± 0.4 points in the low-dose group and −0.2 ± 0.4 points in the high-dose group at 12 months compared with baseline (Table S3; Figure S1B).

Detailed baseline and 12-month comparisons are presented in Figure S2 and Table S3 for MDS-UPDRS. MDS-UPDRS parts I, II, and IV and total scores improved significantly in low- and high-dose groups. Based on 16 h of waking time in the PD diary, mean daily off time decreased from 7.56 to 3.92 h (−3.64 ± 2.45 h, p = 0.031) in the low-dose group and from 8.41 to 5.40 h (−3.01 ± 2.05 h, p = 0.031) in the high-dose group at 12 months.

Other exploratory efficacy measures, including the Non-Motor Symptoms Scale (NMSS), the PD Questionnaire (PDQ-39), and the Schwab and England Activities of Daily Living (SE-ADL) scores, also improved from baseline to 12 months in both groups (Figures S3A–S3F).

Cognitive function, assessed by the Mini-Mental State Examination (MMSE) and the Montreal Cognitive Assessment (MoCA) scores, showed no significant changes over 12 months (Figures S3G and S3H). Although medication adjustments were permitted in cases of motor complications during the follow-up period, levodopa equivalent daily dose (LEDD) remained stable

Table 3. Summary of AEs during the 12-month follow-up period

	Low-dose (n = 6)	High-dose (n = 6)	Total (n = 12)
No. of events			
TEAEs[a]	–	–	–
(1) Mild	4	4	8
(2) Moderate	9	12	21
(3) Severe[b]	1	2	3
(4) Life-threatening or (5) death	0	0	0
No. of participants (%)			
TEAEs[c]	–	–	–
Related to transplanted cells	0	0	0
Related to surgery	0	1 (16.7)	1 (8.3)
Related to immunosuppressants	1 (16.7)	1 (16.7)	2 (16.7)
TESAE[d]	0	1 (16.7)	1 (8.3)
Abnormal overgrowth or tumor formation[e]	0	0	0
CNS inflammation/infection[e]	0	0	0

TEAEs, treatment-emergent adverse events; TESAE, treatment-emergent serious adverse event; CNS, central nervous system.
[a]TEAEs were graded on a scale from 1 to 5 according to the NCI CTCAE, version 5.0. A total of 32 AEs were recorded, all of which were unrelated to the investigational product, A9-DPC.
[b]Three grade 3 events were reported: transient hyperkalemia, a single episode of syncope, and idiopathic thrombocytopenia.
[c]The relationship of TEAEs to transplanted cells, surgery, or immunosuppressants was assessed by investigators. One event, an asymptomatic hemorrhage, was associated with the surgical procedure. Three events were considered possibly related to immunosuppressants: transient hyperkalemia in one participant and idiopathic thrombocytopenia and new-onset diabetes mellitus in the other participant.
[d]A single TESAE occurred in one participant, presenting as thrombocytopenia that remained asymptomatic and required no intervention. The event was classified as a TESAE due to a 1-day extension of hospitalization.
[e]No abnormal cell overgrowth, tumor formation, immune reactions, or infections associated with intracerebral cell transplantation were detected. Assessments of CNS status were based on brain MRI, ^{18}F-FDG PET, laboratory studies, and clinical evaluations by investigators.

over 12 months in both groups (Figure S3I). Detailed LEDD values at each time point are shown in Table S4.

Exploratory imaging outcomes

The brain MRI scans performed postoperatively revealed no evidence of tumor formation or inflammatory reactions at the transplantation sites (Figures S4A and S4B). Expected signal changes along the needle trajectory and near the injection site were noted, confirming the precise transplantation of cells into the putamen (Figures S4A and S4B). An ^{18}F-FDG PET scan at 12 months postoperatively showed no evidence of abnormal overgrowth or ectopic migration of the grafted cells (data not shown).

To assess survival and functional integration of grafted cells, serial ^{18}F-FP-CIT PET imaging was performed at baseline and 12 months after transplantation. The mean ^{18}F-FP-CIT specific binding ratios (SBRs) across patients are presented in Figures 4A and 4B, and individual-level changes in SBRs for all 12 patients are shown in Figure S4C. The SBR values in the bilateral caudate nucleus declined over 12 months compared with the baseline, with a median percentage change of −9.5% (IQR, −11.8 to −1.4) in the low-dose group and −8.8% (IQR, −11.2 to −5.2) in the high-dose group (Figure 4C). The median percentage changes of SBR values in the anterior putamen were −3.0% (IQR, −6.3 to 0.8) in the low-dose group and −0.2% (IQR, −1.5 to 1.9) in the high-dose group. In the posterior putamen, the change of SBR was 1.0% (IQR, −2.1 to 9.3) in the low-dose group and 10.7% (IQR, 5.9–15.0) in the high-dose group (p = 0.065) with a significant between-group difference in the posterior dorsal putamen (p = 0.041) (Figure 4C; Table S5). Notably, increased SBR values in the posterior dorsal putamen on the side showing a more favorable change from baseline were significantly correlated with improvements in the MDS-UPDRS part III (OFF) score, excluding the tremor subscore (Spearman's $\rho = -0.594$, p = 0.046) (Figure S5).

Together, these imaging findings support the anatomical accuracy, survival, and functional integration of the grafted A9-DPC, particularly in the posterior dorsal putamen, where increased dopamine transporter (DAT) activity was associated with clinical motor improvement. The regional specificity of ^{18}F-FP-CIT PET signal changes and their correlation with symptom improvement provide biologically meaningful evidence of DA reinnervation following transplantation.

DISCUSSION

This single-center, open-label, dose-escalation, phase 1/2a trial showed that intra-putamen engraftment of hESC-derived A9-DPC was generally safe and tolerable in moderate-to-severe PD patients with more than 5 years from formal diagnosis.

The safety profile was favorable, with no tumorigenesis, overgrowth of transplanted cells, ectopic cell migration, or immune-mediated inflammation observed.[3] The surgical procedures

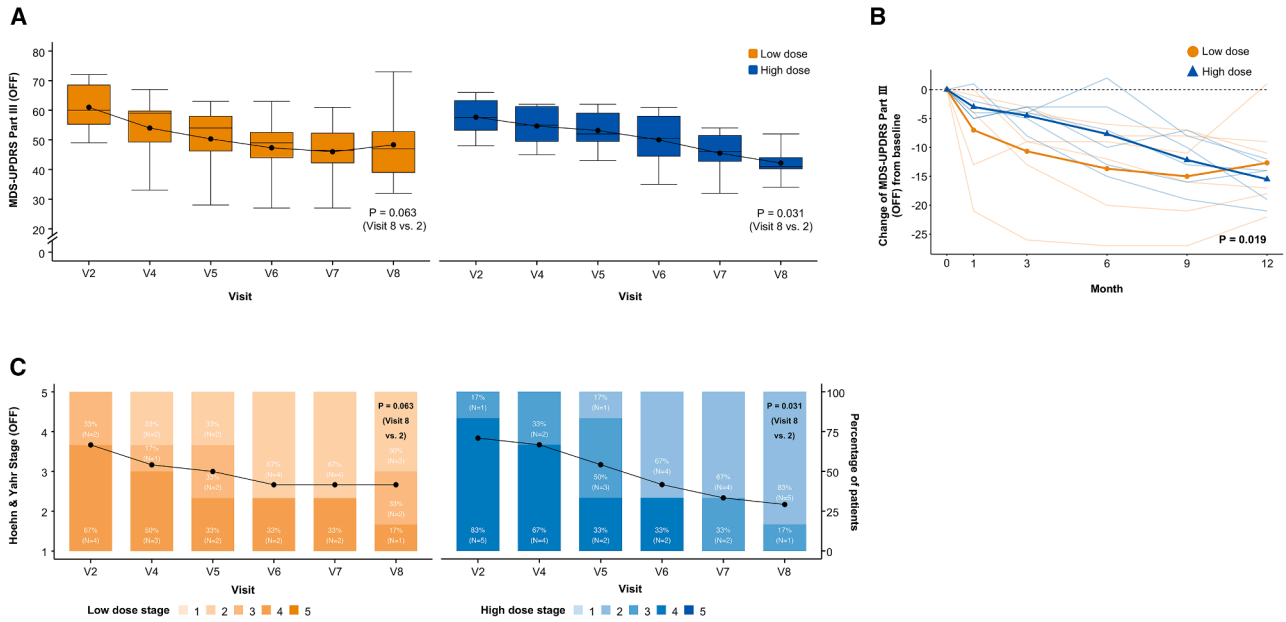

Figure 3. Longitudinal changes in clinical outcomes following transplantation of A9-DPC

(A) MDS-UPDRS part III scores in the off-medication state (OFF). Scores for the low-dose and high-dose groups are shown at baseline and each post-transplantation visit. Scores on MDS-UPDRS part III (OFF) range from 0 to 132, with higher scores indicating greater impairment on a clinician-conducted motor examination. Black dots represent mean values at each visit, and solid lines connect these means across time points. Boxplots are used to present medians (horizontal lines), interquartile ranges (IQRs, boxes), and ranges (whiskers). *p* values were calculated for comparisons between baseline and 12 months using the Wilcoxon signed-rank test. A break in the *y* axis indicates a discontinuity in scale.

(B) Linear mixed-effects model analysis of MDS-UPDRS part III (OFF) scores following transplantation of A9-DPC. Mean changes in the MDS-UPDRS part III (OFF) from baseline to 12 months are shown. Changes were assessed at 1, 3, 6, 9, and 12 months following transplantation. Mean trajectories of MDS-UPDRS part III (OFF) scores are shown for the low-dose and high-dose groups. Solid lines indicate group means, and thin lines indicate individual patient trajectories. Negative values indicate symptomatic improvement. *p* value indicates the statistical significance of the group × time interaction term in a linear mixed-effects model, testing whether the longitudinal trajectories differ between groups (low-dose vs. high-dose).

(C) H&Y stages in the off-medication state. H&Y (OFF) stages are shown for the low-dose and high-dose groups at baseline and each follow-up visit. The H&Y stage ranges from 1 to 5, with higher stages indicating more severe motor impairment. Black dots represent mean values at each visit, and solid lines connect these means across time points. Stacked bar graphs display the distribution of patients across stages at each visit, with the percentage and number of patients indicated within each bar. *p* values were calculated for comparisons between baseline and 12 months using the Wilcoxon signed-rank test.

See also Figures S1–S3 and Tables S3 and S4.

were performed with high precision, achieving targeting accuracy within 1 mm of the intended coordinates. Among 72 stereotactic trajectories, only one asymptomatic intracerebral hemorrhage (1.39%) in the right caudate was observed. This hemorrhage rate is consistent with the procedural risks associated with individual stereotactic trajectories and likely resulted from inadvertent injury to a microscopic vessel.[20,21] No other surgical complications were observed. Three AEs possibly related to immunosuppression were reported: transient hyperkalemia, new-onset diabetes mellitus, and thrombocytopenia. Both hyperkalemia and diabetes mellitus resolved with treatment, while thrombocytopenia improved without intervention and remained asymptomatic. Although no transplanted cell-related complications occurred, these AEs were clearly linked to the therapeutic procedure, including one associated with surgery and three potentially related to immunosuppressants. This indicates the need to carefully monitor perioperative safety, particularly regarding surgical and immunosuppressive risks, in future studies. Importantly, all AEs were transient or controllable, and no serious complications or long-term sequelae occurred. These findings are consistent with preclinical studies of A9-DPC transplantation and underscore the feasibility and safety of intracerebral delivery of these cells.[16]

The findings for efficacy results suggest that A9-DPC transplantation may confer clinically meaningful benefits in patients with PD. First, 11 of 12 participants (91.7%) showed improvements (decrease) in off-medication MDS-UPDRS part III scores and H&Y stage at 12 months. The remaining participant in the low-dose group exhibited only a 1-point increase in MDS-UPDRS part III (OFF) score, which is less than the expected annual progression based on the natural progression of the disease.[22] Second, motor complications were reduced, as indicated by improvements in MDS-UPDRS part IV scores and a decrease in daily off time reported in PD diaries. Third, participants showed significant gains in non-motor and motor aspects of daily living (MDS-UPDRS parts I and II), NMSS, ADL (SE-ADL), and quality of life (PDQ-39). Collectively, these results may support the potential of bilateral putamen transplantation of A9-DPC, leading to motor improvement in the off-medication state, reduction in off time, and improvements in quality of life.

These clinical benefits were supported by PET imaging results. Follow-up ^{18}F-FP-CIT PET imaging showed increased putamen

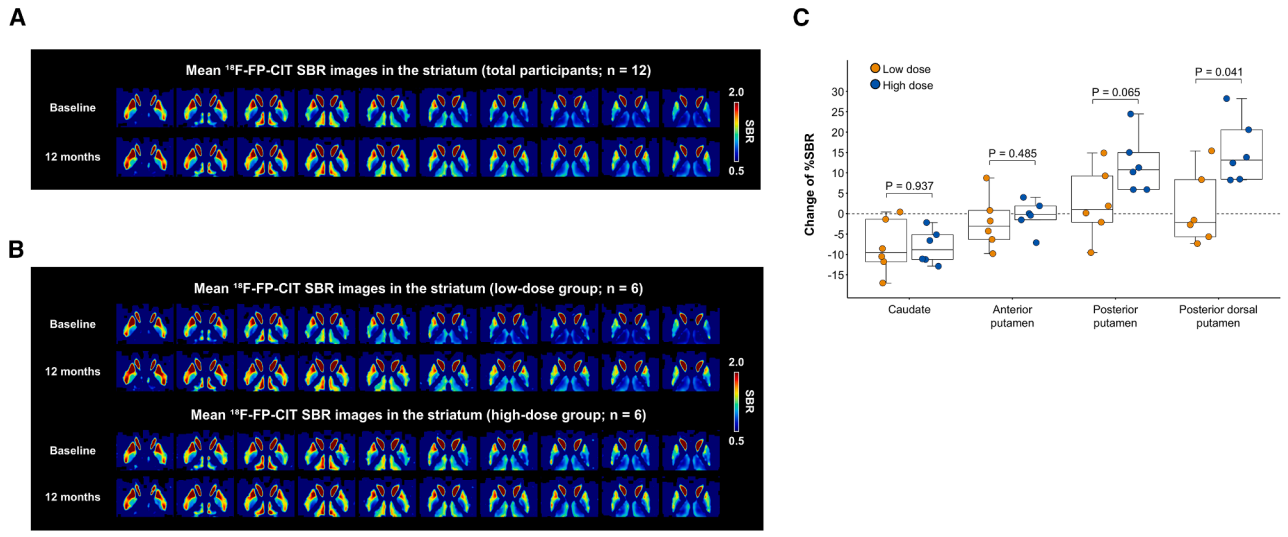

Figure 4. ^{18}F-FP-CIT SBRs at baseline and 12 months after A9-DPC transplantation

(A) ^{18}F-FP-CIT SBR images in the striatum. Axial images of mean ^{18}F-FP-CIT SBRs are shown for all participants (n = 12) at baseline and 12 months after A9-DPC transplantation. SBR images were generated using cerebellar gray matter as the reference tissue. The SBR was calculated by dividing the difference between uptake values in each voxel and the reference region by the uptake value in the reference region.

(B) Group-averaged ^{18}F-FP-CIT SBR images at baseline and 12 months after A9-DPC transplantation. Axial images of mean ^{18}F-FP-CIT SBRs at baseline and 12 months after transplantation are shown for the low-dose group and the high-dose group. SBR images were generated using cerebellar gray matter as the reference tissue. The SBR was calculated by dividing the difference between uptake values in each voxel and the reference region by the uptake value in the reference region.

(C) Regional change of ^{18}F-FP-CIT SBRs. Percentage changes of SBRs from baseline to 12 months are shown for the low-dose and high-dose groups in each subregion. Boxplots show medians (horizontal lines), IQRs (boxes), and full ranges (whiskers), and individual patient values are overlaid. p values were calculated using the Wilcoxon rank-sum test for between-group comparisons.

See also Figures S4–S6 and Table S5.

uptake at the grafted sites, indicative of graft survival, DA neuronal maturation, and synaptic reinnervation. Theoretically, ^{18}F-FP-CIT PET measures synaptic DAT expression,[23] and thus, the observed increase in ^{18}F-FP-CIT PET uptake offers strong evidence of successful graft integration and synaptic recovery. Additionally, increased SBR values in the posterior dorsal putamen on the side with a more favorable change from baseline were significantly correlated with improvements in MDS-UPDRS part III (OFF) scores (excluding tremor), which underscores the functional relevance between graft-derived reinnervation and motor behavior. It is explainable that tremor is not significantly associated with nigral dopamine depletion, and unilateral dopamine change can affect bilateral motor symptoms.[24–27] Collectively, the alignment of improved motor symptoms with increased SBR values in the posterior dorsal putamen suggests that A9-DPC transplantation may contribute to functional reinnervation at the synaptic level, providing mechanistic support for its potential therapeutic effects in PD. This notion is supported by immunocytochemical analyses of rat brain sections from our previous preclinical study.[16] At 24 weeks post-transplantation, we identified grafted DA neurons by their co-expression of human nuclear antigen (HNA) and tyrosine hydroxylase (TH), indicating the successful maturation of A9-DPC into DA neurons (Figure S6A). Furthermore, human-specific synaptophysin signals were exclusively observed in the striatum ipsilateral to the graft (Figures S6B and S6C) but not in the contralateral striatum (Figure S6D). Notably, we found human-specific synaptophysin puncta on the graft-derived TH$^+$ fibers, located in close proximity to dopamine- and cyclic AMP (cAMP)-regulated phosphoprotein of 32 kDa (DARPP-32)-positive host medium spiny neurons (Figure S6C). This finding suggests potential synaptic output from the graft-derived neurons to the host targets. However, definitive confirmation of these connections in the human brain will ultimately require long-term follow-up and detailed postmortem histological examination.

Despite these noteworthy findings, the efficacy results should be interpreted with caution, particularly given the potential variability in MDS-UPDRS part III score owing to motor fluctuations and the placebo effect, as well as the limitations of H&Y stage as an efficacy measure. Beyond the limitations of the assessment tools, the study with a small sample and an open-label, non-randomized design also necessitates careful interpretation of the observed outcomes. The limited sample size was determined based on regulatory and ethical considerations for first-in-human, intracerebral transplantation, and early-phase cell therapy trials, which prioritize safety and feasibility over statistical power for efficacy. Nevertheless, exploratory analyses were pre-specified and conducted under standardized conditions to identify potential efficacy signals and inform the design of future trials. Along with the small sample size, the lack of a control group in this open-label design limits the ability to draw definitive conclusions about efficacy due to the potential influence of the placebo response. An *in vivo* PET study demonstrated that placebo treatment in PD patients led to the release of substantial amounts of dopamine in the

caudate and putamen.[28] However, the patterns of changes in DAT binding in our study seem to be subregion-dependent, showing decreased DAT binding in the caudate that is similar to the annual decline of DAT binding seen in patients with PD[29,30] and increased DAT binding in the posterior putamen (the grafted site). By contrast, in two longitudinal ^{18}F-FP-CIT PET studies,[29,31] none of the 162 individuals with PD showed an increase in DAT binding in the putamen over time. Furthermore, the placebo groups also demonstrated progressive reductions in DAT binding of the putamen in two clinical trials evaluating the therapeutic efficacy of anti-α-synuclein antibodies.[32,33] These findings collectively suggest that an increase in DAT binding on longitudinal imaging in this study is highly unlikely to be attributable to the placebo effect. Clinically, motor improvements in the MDS-UPDRS part III (OFF) score in our patients may exceed placebo-induced motor benefits, where there was an average improvement of 4.3 points with a 95% confidence interval of 3.1–5.6 in the UPDRS part III (OFF) scores for 11.3 months.[34] In future trials, a double-blind, placebo-controlled, multi-center trial with a large sample should be considered to minimize these biases.

Although two previous double-blind, placebo-controlled trials using fetal mesencephalic tissue did not demonstrate conclusive evidence of efficacy,[10,11] the trials suggested that the subset of PD patients with younger age ($\leq$60 years old) or less severe motor scores at baseline (UPDRS part III [OFF] score $\leq$ 49) may have a significant beneficial effect on motor improvement. In this study, however, the baseline age of PD patients showed no association with motor improvement after transplantation of A9-DPC, possibly due to the relatively young average age of the patients (60.3 ± 5.0 years). Our findings suggest that subjects presenting with less severe motor deficits at baseline (MDS-UPDRS part III [OFF] score) demonstrate a more robust response to DA cell transplantation compared with those with more significant motor impairment (Figure S5). These findings imply that the degree of baseline motor impairment could potentially influence the therapeutic outcomes and that young patients with less severe parkinsonian symptoms are likely to be more suitable candidates for transplantation, consistent with results from previous studies of fetal tissue transplants.[10,11]

General cognition remained stable over the 12-month follow-up period, supporting the safety and tolerability of both the intervention and the immunosuppressive regimen in terms of cognitive outcomes. This finding is particularly noteworthy considering that long-term use of immunosuppressants, such as tacrolimus and glucocorticoids, has been associated with risk of cognitive decline.[35,36] On the other hand, dopamine replacement therapy has been shown to improve frontal lobe-mediated cognitive functions in patients with PD,[37,38] raising the possibility that DA cell transplantation could also contribute to cognitive benefit by restoring DA input to the associative striatum. However, follow-up ^{18}F-FP-CIT PET studies revealed no increase in ^{18}F-FP-CIT SBR values in the caudate and anterior putamen, which are part of the associative striatum and closely associated with attention, executive, and visuospatial functions in PD.[39] This finding suggests that the transplanted DA cells may not have provided sufficient DA input to these regions to drive measurable cognitive improvements. Importantly, global cognitive screening tools such as the MMSE and MoCA lack sensitivity to detect domain-specific changes. Therefore, detailed neuropsychological assessment is required to comprehensively assess cognitive outcomes following DA cell transplantation.

Although no immune-mediated AEs were observed during the 12-month period under immunosuppression, long-term surveillance beyond immunosuppression withdrawal is essential to determine the durability of graft survival and rule out delayed immune responses. This consideration is particularly important for future trials exploring tapering or cessation of immunosuppressant treatment. In addition, extended follow-up is necessary to determine whether immunological tolerance to allogeneic grafts can be achieved and maintained in the absence of chronic immunosuppression, which would be a crucial step toward broader clinical application. To address this, all participants in the current trial will undergo long-term safety monitoring with assessments extending up to 5 years, including safety and efficacy tests such as laboratory studies, MDS-UPDRS, brain MRI, and ^{18}F-FP-CIT PET.

Recently, two first-in-human clinical trials of hPSC-derived DA progenitor transplantation in PD were reported: the hESC-based bemdaneprocel trial[40] and the iPSC-based trial (Kyoto University).[41] While all these two and our studies share a common therapeutic goal, key differences exist across multiple domains (Table S6). Compared with the bemdaneprocel trial, which used cryopreserved hESC-derived DA progenitors, our study employed freshly prepared cells. This may enhance cell viability and early graft integration, whereas off-the-shelf therapy may offer practical advantages such as rapid availability and reduced variability.[3,30] In contrast with the bemdaneprocel trial, which delivered up to 5.4 million cells into the post-commissural putamen, and the iPSC-based trial, which delivered a higher number of cells (up to 10 million) into specific subregions of the putamen (dorsal and caudal), our trial used a total dose of up to 6.3 million cells with broader anatomical targeting across the entire putamen (anterior, middle, and posterior). Baseline patient characteristics also varied across studies. Our participants had more advanced disease, with higher mean MDS-UPDRS part III scores in the OFF state (59.3 in our trial vs. 46.6 in the bemdaneprocel trial and 50.8 in the iPSC-based trial), longer time since diagnosis (10.5 years vs. 9.0 and 9.8 years, respectively; the last reflects disease duration), and higher baseline LEDD (1,566 mg/day vs. 1,236 and 1,079 mg/day, respectively), suggesting a more treatment-refractory population compared with the other two cohorts.[11] In terms of imaging modalities, we utilized ^{18}F-FP-CIT PET to directly assess synaptic DAT availability, while the other trials used ^{18}F-DOPA PET. DAT is strongly expressed on mature A9-type DA neurons, and therefore, ^{18}F-FP-CIT PET imaging may be more informative than ^{18}F-DOPA imaging, particularly in the early stages after DA cell transplantation, as a reliable early measure of DA cell maturation *in vivo*.[42,43] In addition, ^{18}F-DOPA images can be confounded by DA medications or inflammatory changes in the graft site,[44–47] while levodopa, dopamine agonists, or monoamine oxidase B (MAO-B) inhibitors do not cause a significant occupancy of the DAT binding site.[48] These differences across hESC-based and iPSC-based trials will serve as valuable references for the planning and conduct of future clinical studies using PSCs in PD.

In contrast with device-aided second-line therapies such as DBS, which act through acute modulation of the basal ganglia

circuitry and allow for rapid reduction in DA medication, stem-cell based therapy exerts its effect via a delayed and gradual mechanism. Transplanted DA progenitors require time to engraft and mature into DA neurons. In this study, DA medications were intentionally maintained at stable doses to ensure safety and minimize confounding. Nevertheless, in some patients, modest LEDD reduction was achieved to avoid levodopa-induced dyskinesia with substantial motor improvement on the MDS-UPDRS part III (OFF) score. As the graft continues to mature, greater reductions in medication may become feasible. Importantly, DBS may have a negative impact on axial motor symptoms such as gait or speech as well as cognition, whereas stem-cell based therapy may be free from these issues. These differences between cell therapy and DBS are summarized in Table S7 and highlight the importance of evaluating long-term outcomes beyond the initial 12-month window.

In conclusion, transplantation of A9-DPC into the putamen was well tolerated over 12 months and associated with clinically meaningful improvements in motor function, daily living, and quality of life in patients with moderate-to-severe PD. Larger, blinded, controlled trials are required to confirm the definitive efficacy, long-term safety, and disease-modifying potential of cell replacement therapy.

Limitations of the study

This trial has several limitations. First, the small sample with a single-center study limits the generalizability of the findings and reduces the ability to detect rare AEs. Second, the open-label design precludes definitive conclusions regarding efficacy owing to the lack of a control group and the potential influence of the placebo response. Third, long-term outcomes after immunosuppression withdrawal remain to be determined.[49] Fourth, dyskinesia was not formally assessed, but no disabling or worsening dyskinesias, compatible with graft-induced dyskinesia, were observed in the off-medication state.[50–52] As specific scales such as the Unified Dyskinesia Rating Scale were not implemented in this phase 1/2a trial, future trials should incorporate more rigorous and quantitative assessments to ensure comprehensive monitoring of dyskinesia. Continued long-term follow-up beyond 12 months is essential to fully assess the durability of clinical benefits and the long-term safety of the graft.

RESOURCE AVAILABILITY

Lead contact

Further information and requests for resources and reagents should be directed to and will be fulfilled by the lead contact, Dong-Wook Kim (dwkim2@yuhs.ac).

Materials availability

This study did not generate new, unique reagents.

Data and code availability

Data reported in this paper will be shared by the lead contact upon request.

This paper does not report original code, except for the in-house Python code used to generate group-averaged ^{18}F-FP-CIT SBR images, which is available from the lead contact upon request.

Any additional information required to reanalyze the data reported in this paper is available from the lead contact upon request.

ACKNOWLEDGMENTS

We thank all participants involved in this trial, and especially Ye Eun Sun, Eun Jung Kweon, and Young So Chung for their support. This work was supported by the Korean Fund for Regenerative Medicine (KFRM) grant funded by the Korean Government (the Ministry of Science and ICT, the Ministry of Health & Welfare) (23D0101L1 and RS-2024-00332790) and the National Research Foundation of Korea (NRF) grant funded by the Korean Government (Ministry of Science and ICT) (2022R1A2C2091165 and RS-2023-00208890).

The graphic image was prepared with the artistic support of the Medical Illustration & Design team, part of the Medical Research Support Services at Yonsei University College of Medicine.

S. Biomedics supported the sponsor-initiated trial (SIT).

AUTHOR CONTRIBUTIONS

J.W.C. and P.H.L. served as principal investigators of this trial. J.W.C. served as a neurosurgeon and performed the surgery. K.W.C. assisted with the surgery as a neurosurgeon. M.-Y.J. assisted with cell preparation during the surgery. J.W.C., C.W.P., D.-S.K., D.-Y.H., M.S.K., M.S.C., P.H.L., and D.-W.K. designed the study and contributed to the preparation of the clinical protocol. D.-H.K., C.-Y.P., S.K., I.J., J.K., M.S.C., and D.-W.K. contributed to the preparation of the statistical analysis plan. H.K.N. and C.W.P. were involved in the acquisition of clinical and imaging data. H.K.N., C.W.P., and P.H.L. assessed the safety and clinical outcomes in the trial. J.H.E., S.T.N., K.-S.J., S.K.C., H.-J.H., S.K., J.K., M.S.C., and D.-W.K. performed cell manufacturing, conducted QC, and monitored the entire process of clinical trial material production. M.K. and I.J. performed statistical analysis. C.W.P. wrote the draft of the manuscript under the guidance and direction of D.-W.K. with the support of D.-H.K., S.P., C.-Y.P., H.K.N., K.W.C., J.W.C., and P.H.L. J.W.C., H.K.N., K.W.C., C.W.P., D.-H.K., S.P., C.-Y.P., M.S.K., I.J., M.S.C., P.H.L., and D.-W.K. edited the manuscript.

All authors reviewed and approved the manuscript.

DECLARATION OF INTERESTS

D.-W.K. is the chief technology officer of S. Biomedics Co., Ltd. D.-H.K., C.-Y.P., J.H.E., S.T.N., K.-S.J., M.-Y.J., S.K.C., H.-J.H., S.K., J.K., and M.S.C. are currently employed at S. Biomedics Co., Ltd. J.H.E., S.T.N., M.S.C., and D.-W.K. are the inventors of the patents related to this work. D.-H.K., C.-Y.P., J.H.E., S.T.N., K.-S.J., M.-Y.J., S.K.C., H.-J.H., S.K., D.-Y.H., J.K., M.S.C., and D.-W.K. hold stock or stock options in S. Biomedics Co., Ltd.

STAR★METHODS

Detailed methods are provided in the online version of this paper and include the following:

- KEY RESOURCES TABLE
- EXPERIMENTAL MODEL AND STUDY PARTICIPANT DETAILS
- METHOD DETAILS
  - Trial design
  - Immunosuppressant treatment
  - Cell preparation
  - Surgical procedures
  - Primary and exploratory endpoints
  - Brain imaging
  - ^{18}F-FP-CIT PET analysis
  - Immunohistochemistry
- QUANTIFICATION AND STATISTICAL ANALYSIS
- ADDITIONAL RESOURCES

SUPPLEMENTAL INFORMATION

Supplemental information can be found online at https://doi.org/10.1016/j.cell.2025.09.010.

Received: May 12, 2025
Revised: July 31, 2025
Accepted: September 9, 2025
Published: October 13, 2025

REFERENCES

1. Postuma, R.B., Berg, D., Stern, M., Poewe, W., Olanow, C.W., Oertel, W., Obeso, J., Marek, K., Litvan, I., Lang, A.E., et al. (2015). MDS clinical diagnostic criteria for Parkinson's disease. Mov. Disord. *30*, 1591–1601. https://doi.org/10.1002/mds.26424.
2. Tanner, C.M., and Ostrem, J.L. (2024). Parkinson's Disease. N. Engl. J. Med. *391*, 442–452. https://doi.org/10.1056/NEJMra2401857.
3. Skidmore, S., and Barker, R.A. (2023). Challenges in the clinical advancement of cell therapies for Parkinson's disease. Nat. Biomed. Eng. *7*, 370–386. https://doi.org/10.1038/s41551-022-00987-y.
4. Okano, H. (2025). Clinical trials test the safety of stem-cell therapy for Parkinson's disease. Nature *641*, 853–854. https://doi.org/10.1038/d41586-025-00688-x.
5. Parmar, M., Grealish, S., and Henchcliffe, C. (2020). The future of stem cell therapies for Parkinson disease. Nat. Rev. Neurosci. *21*, 103–115. https://doi.org/10.1038/s41583-019-0257-7.
6. Bjorklund, A., and Kordower, J.H. (2013). Cell therapy for Parkinson's disease: what next? Mov. Disord. *28*, 110–115. https://doi.org/10.1002/mds.25343.
7. Lindvall, O., Rehncrona, S., Gustavii, B., Brundin, P., Astedt, B., Widner, H., Lindholm, T., Björklund, A., Leenders, K.L., Rothwell, J.C., et al. (1988). Fetal dopamine-rich mesencephalic grafts in Parkinson's disease. Lancet *2*, 1483–1484. https://doi.org/10.1016/s0140-6736(88)90950-6.
8. Kefalopoulou, Z., Politis, M., Piccini, P., Mencacci, N., Bhatia, K., Jahanshahi, M., Widner, H., Rehncrona, S., Brundin, P., Björklund, A., et al. (2014). Long-term clinical outcome of fetal cell transplantation for Parkinson disease: two case reports. JAMA Neurol. *71*, 83–87. https://doi.org/10.1001/jamaneurol.2013.4749.
9. Li, W., Englund, E., Widner, H., Mattsson, B., van Westen, D., Lätt, J., Rehncrona, S., Brundin, P., Björklund, A., Lindvall, O., et al. (2016). Extensive graft-derived dopaminergic innervation is maintained 24 years after transplantation in the degenerating parkinsonian brain. Proc. Natl. Acad. Sci. USA *113*, 6544–6549. https://doi.org/10.1073/pnas.1605245113.
10. Freed, C.R., Greene, P.E., Breeze, R.E., Tsai, W.Y., DuMouchel, W., Kao, R., Dillon, S., Winfield, H., Culver, S., Trojanowski, J.Q., et al. (2001). Transplantation of embryonic dopamine neurons for severe Parkinson's disease. N. Engl. J. Med. *344*, 710–719. https://doi.org/10.1056/NEJM200103083441002.
11. Olanow, C.W., Goetz, C.G., Kordower, J.H., Stoessl, A.J., Sossi, V., Brin, M.F., Shannon, K.M., Nauert, G.M., Perl, D.P., Godbold, J., et al. (2003). A double-blind controlled trial of bilateral fetal nigral transplantation in Parkinson's disease. Ann. Neurol. *54*, 403–414. https://doi.org/10.1002/ana.10720.
12. Roy, N.S., Cleren, C., Singh, S.K., Yang, L., Beal, M.F., and Goldman, S.A. (2006). Functional engraftment of human ES cell-derived dopaminergic neurons enriched by coculture with telomerase-immortalized midbrain astrocytes. Nat. Med. *12*, 1259–1268. https://doi.org/10.1038/nm1495.
13. Cho, M.S., Hwang, D.Y., and Kim, D.W. (2008). Efficient derivation of functional dopaminergic neurons from human embryonic stem cells on a large scale. Nat. Protoc. *3*, 1888–1894. https://doi.org/10.1038/nprot.2008.188.
14. Piao, J., Zabierowski, S., Dubose, B.N., Hill, E.J., Navare, M., Claros, N., Rosen, S., Ramnarine, K., Horn, C., Fredrickson, C., et al. (2021). Preclinical Efficacy and Safety of a Human Embryonic Stem Cell-Derived Midbrain Dopamine Progenitor Product, MSK-DA01. Cell Stem Cell *28*, 217–229.e7. https://doi.org/10.1016/j.stem.2021.01.004.
15. Kirkeby, A., Nelander, J., Hoban, D.B., Rogelius, N., Bjartmarz, H., Novo Nordisk Cell Therapy R&D, Storm, P., Fiorenzano, A., Adler, A.F., Vale, S., et al. (2023). Preclinical quality, safety, and efficacy of a human embryonic stem cell-derived product for the treatment of Parkinson's disease, STEM-PD. Cell Stem Cell *30*, 1299–1314.e9. https://doi.org/10.1016/j.stem.2023.08.014.
16. Park, S., Park, C.W., Eom, J.H., Jo, M.Y., Hur, H.J., Choi, S.K., Lee, J.S., Nam, S.T., Jo, K.S., Oh, Y.W., et al. (2024). Preclinical and dose-ranging assessment of hESC-derived dopaminergic progenitors for a clinical trial on Parkinson's disease. Cell Stem Cell *31*, 25–38.e8. https://doi.org/10.1016/j.stem.2023.11.009.
17. Doi, D., Magotani, H., Kikuchi, T., Ikeda, M., Hiramatsu, S., Yoshida, K., Amano, N., Nomura, M., Umekage, M., Morizane, A., et al. (2020). Pre-clinical study of induced pluripotent stem cell-derived dopaminergic progenitor cells for Parkinson's disease. Nat. Commun. *11*, 3369. https://doi.org/10.1038/s41467-020-17165-w.
18. Schweitzer, J.S., Song, B., Herrington, T.M., Park, T.Y., Lee, N., Ko, S., Jeon, J., Cha, Y., Kim, K., Li, Q., et al. (2020). Personalized iPSC-Derived Dopamine Progenitor Cells for Parkinson's Disease. N. Engl. J. Med. *382*, 1926–1932. https://doi.org/10.1056/NEJMoa1915872.
19. Martínez-Martín, P., Rodríguez-Blázquez, C., Mario, A., Arakaki, T., Arillo, V.C., Chaná, P., Fernández, W., Garretto, N., Martínez-Castrillo, J.C., Rodríguez-Violante, M., et al. (2015). Parkinson's disease severity levels and MDS-Unified Parkinson's Disease Rating Scale. Parkinsonism Relat. Disord. *21*, 50–54. https://doi.org/10.1016/j.parkreldis.2014.10.026.
20. Binder, D.K., Rau, G.M., and Starr, P.A. (2005). Risk factors for hemorrhage during microelectrode-guided deep brain stimulator implantation for movement disorders. Neurosurgery *56*, 722–732. https://doi.org/10.1227/01.neu.0000156473.57196.7e.
21. Ben-Haim, S., Asaad, W.F., Gale, J.T., and Eskandar, E.N. (2009). Risk factors for hemorrhage during microelectrode-guided deep brain stimulation and the introduction of an improved microelectrode design. Neurosurgery *64*, 762–763. https://doi.org/10.1227/01.NEU.0000339173.77240.34.
22. Holden, S.K., Finseth, T., Sillau, S.H., and Berman, B.D. (2018). Progression of MDS-UPDRS Scores Over Five Years in De Novo Parkinson Disease from the Parkinson's Progression Markers Initiative Cohort. Mov. Disord. Clin. Pract. *5*, 47–53. https://doi.org/10.1002/mdc3.12553.
23. Kazumata, K., Dhawan, V., Chaly, T., Antonini, A., Margouleff, C., Belakhlef, A., Neumeyer, J., and Eidelberg, D. (1998). Dopamine transporter imaging with fluorine-18-FPCIT and PET. J. Nucl. Med. *39*, 1521–1530.
24. Pirker, W. (2003). Correlation of dopamine transporter imaging with parkinsonian motor handicap: how close is it? Mov. Disord. *18*, S43–S51. https://doi.org/10.1002/mds.10579.
25. Tosin, M.H.S., Goetz, C.G., Luo, S., Choi, D., and Stebbins, G.T. (2020). Item Response Theory Analysis of the MDS-UPDRS Motor Examination: Tremor vs. Nontremor Items. Mov. Disord. *35*, 1587–1595. https://doi.org/10.1002/mds.28110.
26. Luo, S., Zou, H., Goetz, C.G., Choi, D., Oakes, D., Simuni, T., and Stebbins, G.T. (2021). Novel Approach to Movement Disorder Society-Unified Parkinson's Disease Rating Scale Monitoring in Clinical Trials: Longitudinal Item Response Theory Models. Mov. Disord. Clin. Pract. *8*, 1083–1091. https://doi.org/10.1002/mdc3.13311.
27. Peschanski, M., Defer, G., N'Guyen, J.P., Ricolfi, F., Monfort, J.C., Remy, P., Geny, C., Samson, Y., Hantraye, P., and Jeny, R. (1994). Bilateral motor improvement and alteration of L-dopa effect in two patients with Parkinson's disease following intrastriatal transplantation of foetal ventral mesencephalon. Brain *117*, 487–499. https://doi.org/10.1093/brain/117.3.487.
28. de la Fuente-Fernández, R., Ruth, T.J., Sossi, V., Schulzer, M., Calne, D.B., and Stoessl, A.J. (2001). Expectation and dopamine release: mechanism of the placebo effect in Parkinson's disease. Science *293*, 1164–1166. https://doi.org/10.1126/science.1060937.
29. Song, Y., Lee, J.H., Kim, H.K., Lee, J.H., Ryu, Y.H., Yoo, H.S., and Lyoo, C.H. (2025). Longitudinal Trajectory of Dopamine and Serotonin Transporters in Parkinson Disease. J. Nucl. Med. *66*, 286–292. https://doi.org/10.2967/jnumed.124.268365.

30. Marek, K., Innis, R., van Dyck, C., Fussell, B., Early, M., Eberly, S., Oakes, D., and Seibyl, J. (2001). [123I]beta-CIT SPECT imaging assessment of the rate of Parkinson's disease progression. Neurology *57*, 2089–2094. https://doi.org/10.1212/wnl.57.11.2089.

31. Sung, C., Lee, J.H., Oh, J.S., Oh, M., Lee, S.J., Oh, S.J., Chung, S.J., Lee, C.S., and Kim, J.S. (2017). Longitudinal Decline of Striatal Subregional [^{18}F]FP-CIT Uptake in Parkinson's Disease. Nucl. Med. Mol. Imaging *51*, 304–313. https://doi.org/10.1007/s13139-017-0481-x.

32. Pagano, G., Taylor, K.I., Anzures-Cabrera, J., Marchesi, M., Simuni, T., Marek, K., Postuma, R.B., Pavese, N., Stocchi, F., Azulay, J.P., et al. (2022). Trial of Prasinezumab in Early-Stage Parkinson's Disease. N. Engl. J. Med. *387*, 421–432. https://doi.org/10.1056/NEJMoa2202867.

33. Lang, A.E., Siderowf, A.D., Macklin, E.A., Poewe, W., Brooks, D.J., Fernandez, H.H., Rascol, O., Giladi, N., Stocchi, F., Tanner, C.M., et al. (2022). Trial of Cinpanemab in Early Parkinson's Disease. N. Engl. J. Med. *387*, 408–420. https://doi.org/10.1056/NEJMoa2203395.

34. Polgar, S., Buultjens, M., Wijeratne, T., Finkelstein, D.I., Mohamed, S., and Karimi, L. (2022). The Placebo Response in Double-Blind Randomised Trials Evaluating Regenerative Therapies for Parkinson's Disease: A Systematic Review and Meta-Analysis. J. Parkinsons Dis. *12*, 759–771. https://doi.org/10.3233/JPD-212610.

35. Thiankhaw, K., Chattipakorn, N., and Chattipakorn, S.C. (2024). How calcineurin inhibitors affect cognition. Acta Physiol. (Oxf.) *240*, e14161. https://doi.org/10.1111/apha.14161.

36. Spannenburg, L., and Reed, H. (2023). Adverse cognitive effects of glucocorticoids: A systematic review of the literature. Steroids *200*, 109314. https://doi.org/10.1016/j.steroids.2023.109314.

37. Cools, R. (2006). Dopaminergic modulation of cognitive function-implications for L-DOPA treatment in Parkinson's disease. Neurosci. Biobehav. Rev. *30*, 1–23. https://doi.org/10.1016/j.neubiorev.2005.03.024.

38. Miah, I.P., Olde Dubbelink, K.T., Stoffers, D., Deijen, J.B., and Berendse, H.W. (2012). Early-stage cognitive impairment in Parkinson's disease and the influence of dopamine replacement therapy. Eur. J. Neurol. *19*, 510–516. https://doi.org/10.1111/j.1468-1331.2011.03578.x.

39. Chung, S.J., Yoo, H.S., Oh, J.S., Kim, J.S., Ye, B.S., Sohn, Y.H., and Lee, P.H. (2018). Effect of striatal dopamine depletion on cognition in de novo Parkinson's disease. Parkinsonism Relat. Disord. *51*, 43–48. https://doi.org/10.1016/j.parkreldis.2018.02.048.

40. Tabar, V., Sarva, H., Lozano, A.M., Fasano, A., Kalia, S.K., Yu, K.K.H., Brennan, C., Ma, Y., Peng, S., Eidelberg, D., et al. (2025). Phase I trial of hES cell-derived dopaminergic neurons for Parkinson's disease. Nature *641*, 978–983. https://doi.org/10.1038/s41586-025-08845-y.

41. Sawamoto, N., Doi, D., Nakanishi, E., Sawamura, M., Kikuchi, T., Yamakado, H., Taruno, Y., Shima, A., Fushimi, Y., Okada, T., et al. (2025). Phase I/II trial of iPS-cell-derived dopaminergic cells for Parkinson's disease. Nature *641*, 971–977. https://doi.org/10.1038/s41586-025-08700-0.

42. Goggi, J.L., Qiu, L., Liao, M.C., Khanapur, S., Jiang, L., Boominathan, R., Hartimath, S.V., Cheng, P., Yong, F.F., Soh, V., et al. (2020). Dopamine transporter neuroimaging accurately assesses the maturation of dopamine neurons in a preclinical model of Parkinson's disease. Stem Cell Res. Ther. *11*, 347. https://doi.org/10.1186/s13287-020-01868-4.

43. Kikuchi, T., Morizane, A., Doi, D., Onoe, H., Hayashi, T., Kawasaki, T., Saiki, H., Miyamoto, S., and Takahashi, J. (2011). Survival of human induced pluripotent stem cell-derived midbrain dopaminergic neurons in the brain of a primate model of Parkinson's disease. J. Parkinsons Dis. *1*, 395–412. https://doi.org/10.3233/JPD-2011-11070.

44. Torstenson, R., Hartvig, P., Långström, B., Westerberg, G., and Tedroff, J. (1997). Differential effects of levodopa on dopaminergic function in early and advanced Parkinson's disease. Ann. Neurol. *41*, 334–340. https://doi.org/10.1002/ana.410410308.

45. Kumakura, Y., Danielsen, E.H., Reilhac, A., Gjedde, A., and Cumming, P. (2004). Levodopa effect on [18F]fluorodopa influx to brain: normal volunteers and patients with Parkinson's disease. Acta Neurol. Scand. *110*, 188–195. https://doi.org/10.1111/j.1600-0404.2004.00299.x.

46. Sala, Q., Metellus, P., Taieb, D., Kaphan, E., Figarella-Branger, D., and Guedj, E. (2014). 18F-DOPA, a clinically available PET tracer to study brain inflammation? Clin. Nucl. Med. *39*, e283–e285. https://doi.org/10.1097/RLU.0000000000000383.

47. Dadone-Montaudié, B., Ambrosetti, D., Dufour, M., Darcourt, J., Almairac, F., Coyne, J., Virolle, T., Humbert, O., and Burel-Vandenbos, F. (2017). [18F] FDOPA standardized uptake values of brain tumors are not exclusively dependent on LAT1 expression. PLoS One *12*, e0184625. https://doi.org/10.1371/journal.pone.0184625.

48. Chahid, Y., Sheikh, Z.H., Mitropoulos, M., and Booij, J. (2023). A systematic review of the potential effects of medications and drugs of abuse on dopamine transporter imaging using [^{123}I]I-FP-CIT SPECT in routine practice. Eur. J. Nucl. Med. Mol. Imaging *50*, 1974–1987. https://doi.org/10.1007/s00259-023-06171-x.

49. Barker, R.A.; TRANSEURO consortium (2019). Designing stem-cell-based dopamine cell replacement trials for Parkinson's disease. Nat. Med. *25*, 1045–1053. https://doi.org/10.1038/s41591-019-0507-2.

50. Greene, P.E., Fahn, S., Eidelberg, D., Bjugstad, K.B., Breeze, R.E., and Freed, C.R. (2021). Persistent dyskinesias in patients with fetal tissue transplantation for Parkinson disease. NPJ Parkinsons Dis. *7*, 38. https://doi.org/10.1038/s41531-021-00183-w.

51. Olanow, C.W., Gracies, J.M., Goetz, C.G., Stoessl, A.J., Freeman, T., Kordower, J.H., Godbold, J., and Obeso, J.A. (2009). Clinical pattern and risk factors for dyskinesias following fetal nigral transplantation in Parkinson's disease: a double blind video-based analysis. Mov. Disord. *24*, 336–343. https://doi.org/10.1002/mds.22208.

52. Hagell, P., Piccini, P., Björklund, A., Brundin, P., Rehncrona, S., Widner, H., Crabb, L., Pavese, N., Oertel, W.H., Quinn, N., et al. (2002). Dyskinesias following neural transplantation in Parkinson's disease. Nat. Neurosci. *5*, 627–628. https://doi.org/10.1038/nn863.

53. Storer, B.E. (1989). Design and analysis of phase I clinical trials. Biometrics *45*, 925–937. https://doi.org/10.2307/2531693.

54. Margreiter, R.; European Tacrolimus vs Ciclosporin Microemulsion Renal Transplantation Study Group (2002). Efficacy and safety of tacrolimus compared with ciclosporin microemulsion in renal transplantation: a randomised multicentre study. Lancet *359*, 741–746. https://doi.org/10.1016/S0140-6736(02)07875-3.

55. Nashan, B., Moore, R., Amlot, P., Schmidt, A.G., Abeywickrama, K., and Soulillou, J.P. (1997). Randomised trial of basiliximab versus placebo for control of acute cellular rejection in renal allograft recipients. CHIB 201 International Study Group. Lancet *350*, 1193–1198. https://doi.org/10.1016/s0140-6736(97)09278-7.

56. Leonardi, G., Messina, M., Giraudi, R., Pellu, V., Fop, F., and Segoloni, G. P. (2004). Basiliximab in association with tacrolimus and steroids in caucasian cadaveric renal transplanted patients: significant decrease in early acute rejection rate and hospitalization time. Clin. Transplant. *18*, 113–118. https://doi.org/10.1046/j.1399-0012.2003.00150.x.

57. Goetz, C.G., Tilley, B.C., Shaftman, S.R., Stebbins, G.T., Fahn, S., Martinez-Martin, P., Poewe, W., Sampaio, C., Stern, M.B., Dodel, R., et al. (2008). Movement Disorder Society-sponsored revision of the Unified Parkinson's Disease Rating Scale (MDS-UPDRS): scale presentation and clinimetric testing results. Mov. Disord. *23*, 2129–2170. https://doi.org/10.1002/mds.22340.

58. Ahn, H.J., Chin, J., Park, A., Lee, B.H., Suh, M.K., Seo, S.W., and Na, D.L. (2010). Seoul Neuropsychological Screening Battery-dementia version (SNSB-D): a useful tool for assessing and monitoring cognitive impairments in dementia patients. J. Korean Med. Sci. *25*, 1071–1076. https://doi.org/10.3346/jkms.2010.25.7.1071.

59. Kim, J.I., Sunwoo, M.K., Sohn, Y.H., Lee, P.H., and Hong, J.Y. (2016). The MMSE and MoCA for Screening Cognitive Impairment in Less Educated Patients with Parkinson's Disease. J. Mov. Disord. *9*, 152–159. https://doi.org/10.14802/jmd.16020.

60. Fischl, B., Salat, D.H., Busa, E., Albert, M., Dieterich, M., Haselgrove, C., van der Kouwe, A., Killiany, R., Kennedy, D., Klaveness, S., et al. (2002). Whole brain segmentation: automated labeling of neuroanatomical structures in the human brain. Neuron *33*, 341–355. https://doi.org/10.1016/s0896-6273(02)00569-x.

61. Oh, M., Kim, J.S., Kim, J.Y., Shin, K.H., Park, S.H., Kim, H.O., Moon, D.H., Oh, S.J., Chung, S.J., and Lee, C.S. (2012). Subregional patterns of preferential striatal dopamine transporter loss differ in Parkinson disease, progressive supranuclear palsy, and multiple-system atrophy. J. Nucl. Med. *53*, 399–406. https://doi.org/10.2967/jnumed.111.095224.

62. Mawlawi, O., Martinez, D., Slifstein, M., Broft, A., Chatterjee, R., Hwang, D. R., Huang, Y., Simpson, N., Ngo, K., Van Heertum, R., et al. (2001). Imaging human mesolimbic dopamine transmission with positron emission tomography: I. Accuracy and precision of D(2) receptor parameter measurements in ventral striatum. J. Cereb. Blood Flow Metab. *21*, 1034–1057. https://doi.org/10.1097/00004647-200109000-00002.

63. Rousset, O.G., Ma, Y., and Evans, A.C. (1998). Correction for partial volume effects in PET: principle and validation. J. Nucl. Med. *39*, 904–911.

64. Rousset, O.G., Collins, D.L., Rahmim, A., and Wong, D.F. (2008). Design and implementation of an automated partial volume correction in PET: application to dopamine receptor quantification in the normal human striatum. J. Nucl. Med. *49*, 1097–1106. https://doi.org/10.2967/jnumed.107.048330.

65. Thomas, B.A., Erlandsson, K., Modat, M., Thurfjell, L., Vandenberghe, R., Ourselin, S., and Hutton, B.F. (2011). The importance of appropriate partial volume correction for PET quantification in Alzheimer's disease. Eur. J. Nucl. Med. Mol. Imaging *38*, 1104–1119. https://doi.org/10.1007/s00259-011-1745-9.

66. Kish, S.J., Furukawa, Y., Chang, L.J., Tong, J., Ginovart, N., Wilson, A., Houle, S., and Meyer, J.H. (2005). Regional distribution of serotonin transporter protein in postmortem human brain: is the cerebellum a SERT-free brain region? Nucl. Med. Biol. *32*, 123–128. https://doi.org/10.1016/j.nucmedbio.2004.10.001.

STAR★METHODS

KEY RESOURCES TABLE

REAGENT or RESOURCE	SOURCE	IDENTIFIER
Antibodies		
GFAP	Millipore Sigma	Cat#MAB360; RRID:AB_11212597
PAX6	Santa Cruz	Cat#sc-81649; RRID:AB_1127044
hSYP	Thermo Fisher Scientific	Cat#14-6525-82; RRID:AB_10670280
TH	Pel-freez	Cat#P60101; RRID:AB_461070
DARPP-32	Thermo Fisher Scientific	Cat#MA5-14968; RRID:AB_10981784
Alexa 488 anti-HNA	Millipore Sigma	Cat#MAB1281A; RRID:AB_94090
Alexa 488 anti-FOXA2	R&D Systems	Cat#IC2400G; RRID:AB_2801552
Alexa 647 anti-βIII-Tubulin	BioLegend	Cat#801210; RRID:AB_2686931
Chemicals, Peptides, and Recombinant Proteins		
WebTrix™ T25 flask	Amolifescience	Cat#AL-T-100025
Y27632	Millipore Sigma	Cat#688000-100MG
Dulbecco's Modified Eagle Medium, Nutrient Mixture F-12	Thermo Fisher Scientific	Cat#11320-033
CTS™ N-2 supplement	Thermo Fisher Scientific	Cat#A13707-01
B-27™ supplement, XenoFree	Thermo Fisher Scientific	Cat#A14867-01
Accutase	Millipore Sigma	Cat#SCR005
Critical Commercial Assays		
GAPDH Taqman assay	Thermo Fisher Scientific	ID: Hs99999905_m1
NANOG Taqman assay	Thermo Fisher Scientific	ID: Hs02387400_g1
REX1 Taqman assay	Thermo Fisher Scientific	ID: Hs00399279_m1
TDGF1 Taqman assay	Thermo Fisher Scientific	ID: Hs02339499_g1
Experimental Models: Cell Lines		
SNU-hES32	Seoul National University	RRID:CVCL_L118
Oligonucleotides		
FOXA2 forward primer	Cosmo Genetech	CCG TTC TCC ATC AAC CT
FOXA2 reverse primer	Cosmo Genetech	GGG GTA GTG CAT CAC CTG TT
TUBB3 forward primer	Cosmo Genetech	AGT CGC CCA CGT AGT TGC
TUBB3 reverse primer	Cosmo Genetech	CGC CCA GTA TGA GGG AGA T
GAPDH forward primer	Cosmo Genetech	CAA TGA CCC CTT CAT TGA CC
GAPDH reverse primer	Cosmo Genetech	TTG ATT TTG GAG GGA TCT CG
Software and Algorithms		
DxFLEX™ software (version 2.0)	Beckman Coulter	N/A
StealthStation™ S8	Medtronic	N/A
Brainlab Elements	Brainlab	N/A
FreeSurfer	Massachusetts General Hospital	RRID:SCR_001847
Statistical Parametric Mapping 12	Wellcome Trust Centre for Neuroimaging, University College London	RRID:SCR_007037
Statistical Analysis System (version 9.4)	SAS Institute	RRID:SCR_008567
Python	Python Software Foundation	RRID:SCR_008394

EXPERIMENTAL MODEL AND STUDY PARTICIPANT DETAILS

This single-center, open-label, dose-escalation phase 1/2a clinical trial was conducted at Severance Hospital, Yonsei University College of Medicine, Seoul, Korea, to evaluate the safety and exploratory efficacy of allogenic hESC-derived DA progenitors in patients with PD, and was conducted in accordance to the Clinical Study Protocol (Methods S1). This trial was approved by the institutional review board and the MFDS, conducted according to the principles of the Declaration of Helsinki and Good Clinical Practice guidelines, and registered at ClinicalTrials.gov (NCT05887466). All patients provided written informed consent. The sponsor, S. Biomedics, provided the investigational product (A9-DPC), conducted data analyses, and funded the study. Participants were enrolled based on the inclusion and exclusion criteria specified in the attached clinical study protocol (Methods S1). Briefly, eligible participants were 50 to 75 years of age with idiopathic PD of more than 5 years' duration and without dementia. Additional criteria included a minimum 40% motor improvement following levodopa challenge, a H&Y stage of 3 or 4 in the off-medication state, stable antiparkinsonian medications for at least 3 months before screening, and the presence of motor complications.

Thirteen patients were assessed for eligibility, and one was excluded due to screening failure. Twelve participants were enrolled and assigned to low-dose (3.15 million cells, n = 6) or high-dose (6.30 million cells, n = 6) group according to a 3 + 3 rule-based design.[53] An initial three patients underwent low-dose A9-DPC transplantation, and no DLT, defined as a grade 3 or higher adverse event related to treatment according to the NCI CTCAE version 5.0, was observed during the 3-month evaluation period. Following safety review, SRC approved sequential enrollment of three patients in the high-dose group. After another 3-month observation with no DLT, the SRC permitted sequential expansion to three additional patients in each dose group. The low and high cell doses were determined based on preclinical dose–response studies in rat PD models,[16] which estimated the minimum effective therapeutic dose to correspond to 1.87–3.74 million cells per human brain, equivalent to approximately 0.14–0.28 million surviving DA neurons per putamen. This range is consistent with postmortem findings from fetal nigral grafts demonstrating clinical benefit above 0.1 million DA neurons per putamen. Accordingly, 3.15 million cells were selected as the low dose and 6.30 million cells as the high dose for the present clinical trial. Baseline demographic and clinical characteristics are summarized in Table 2, and no significant difference in sex distribution was observed between the low-dose group (83.3% male) and the high-dose group (66.7% male) by Fisher's exact test ($p > 0.999$). Overall, the study included both male and female participants (75% male, 25% female), and all 12 participants were East Asian (Korean). The influence of sex, gender, race, ethnicity or ancestry on the study outcomes could not be determined due to the small sample size and the early-phase design of this trial. This limitation should be considered when generalizing the present findings to broader populations.

METHOD DETAILS

Trial design

Participants were sequentially allocated to low- or high-dose groups following a 3 + 3 rule-based dose-escalation design. Briefly, three participants were initially enrolled at the low-dose group (3.15×10^6 cells). In the absence of DLTs during the first 3 months, three additional participants were enrolled at the high-dose group (6.30×10^6 cells). After a second safety review, three more participants were added to each group, yielding a total of six per cohort. No additional randomization or stratification was applied.

The study was open-label, with no blinding of participants, clinicians, or outcome assessors. Eligibility was determined according to prespecified inclusion and exclusion criteria. Key inclusion criteria were: diagnosis of Parkinson's disease for $\geq$5 years, age 50–75 years, and stable dopaminergic medication for $\geq$3 months. Key exclusion criteria included dementia, atypical parkinsonism, uncontrolled comorbidities, or prior exposure to cell therapies. Full details are provided in the clinical study protocol (Methods S1).

Immunosuppressant treatment

Immunosuppressants included basiliximab, methylprednisolone/prednisolone, and tacrolimus, which were administered for up to 12 months.[40] Basiliximab (20 mg IV) was administered on the day of transplantation and postoperative day 4; methylprednisolone (500 mg IV) was given preoperatively, followed by oral prednisolone taper; and tacrolimus was initiated 2 days before surgery and adjusted to maintain a trough level of 4 to 7 ng/mL.[54–56]

Cell preparation

A clinical-grade hESC line (SNU-hES32), which is available from the Institute of Reproductive Medicine and Population of Seoul National University, was expanded and differentiated into mDA progenitors in a GMP facility (S. Biomedics) as described in detail in our previous preclinical study (Figure 1).[16] All processes were conducted under GMP-compliant conditions with certified reagents and materials under strict QC standards. Briefly, hESCs from the master cell bank were expanded and differentiated into mDA progenitors using a scalable 3D culture system incorporating four small molecules to ensure high purity and reproducibility. On DD 19, cells were cryopreserved to establish the WCB.

Cells from WCB were thawed according to the surgery schedule and cultured for an additional 6 days. On DD 25, cells underwent QC assessments (Table S1).[16] Among the 13 manufactured cell product batches, 12 satisfied the established criteria, whereas one batch (Lot #: ES04-TAP23006) tested positive for mycoplasma and was excluded from clinical use.

After QC tests, the final products (A9-DPC) with isotonic sodium chloride (Dai Han Pharm. Co., Ltd., Seoul, South Korea), total 500 μL, were stocked in 1-mL glass vials (DWK Life Sciences, Millville, NJ, USA). The low-dose group was prepared with a total of 7.0×10^6 cells, while the high-dose group contained 14.0×10^6 cells. After manufacturing, the products were maintained under refrigeration during shipment to ensure the temperature remained within 2–8°C. A thermometer was used to monitor the temperature throughout the transportation process, and A9-DPC was administered into the patient's brain within 36 hours.

Surgical procedures

All participants underwent stereotactic transplantation of allogenic A9-DPC into the bilateral putamen under general anesthesia (Figure S7). The putamen sites were targeted using the Leksell stereotactic frame G (Elekta, Stockholm, Sweden) in conjunction with MRI and stereotactic planning software, Medtronic StealthStation S8 (Medtronic, Minneapolis, MN, USA), and Brainlab Elements (Brainlab, Munich, Germany).

A total of six trajectories (three per hemisphere: anterior, middle, and posterior) were used, each with three injection sites, resulting in 18 deposits per participant. Participants in the low-dose group received 3.15 million cells and those in the high-dose group received 6.30 million cells. Injections were evenly distributed throughout the putamen to ensure optimal coverage. Immediate postoperative CT scan was performed to assess for intracerebral hemorrhage.

Primary and exploratory endpoints

The primary objective of this trial was to evaluate the safety and tolerability of allogenic A9-DPC transplantation in each low-dose and high-dose group. Safety was assessed by the incidence and severity of treatment-emergent AEs and graft-related complications, including intracerebral hemorrhage, infection, immunologic responses to the graft, and neoplastic changes. AEs were coded using the Medical Dictionary for Regulatory Activities version 28.0.

Exploratory clinical endpoints included changes from baseline in MDS-UPDRS part I through IV, and H&Y stage.[57] Additional exploratory measures included NMSS, PDQ-39, and SE-ADL scores. Baseline cognitive status was assessed using the standardized Seoul Neuropsychological Screening Battery.[58] The Korean versions of MMSE and MoCA were administered at baseline and repeated during follow-up assessments.[59] Imaging-based exploratory endpoints included changes in striatal uptake on ^{18}F-FP-CIT PET.

Brain imaging

MRI scans, including T1-weighted, fluid-attenuated inversion recovery (FLAIR), and gadolinium-enhanced T1-weighted sequences, were acquired using a 3.0-T Ingenia CX scanner (Philips Medical System, Best, the Netherlands) with a 32-channel head coil. High-resolution, T1-weighted images were obtained using a 3D fast field echo sequence with the following parameters: acquisition matrix of 240×240; 180 sagittal slices; field of view, 240 mm; voxel size, $1.0 \times 1.0 \times 1.0$ mm^3; echo time, 4.6 milliseconds; repetition time, 9.6 milliseconds; flip angle, 9°; and no interslice gap. Imaging guidance for the surgical procedure was performed with a 3.0-T Discovery MR750 scanner (GE Healthcare, Chicago, IL, USA).

^{18}F-FP-CIT PET/CT and ^{18}F-FDG PET/CT scans were performed using a Discovery 600 system (GE Healthcare, Milwaukee, WI, USA). Subjects fasted for at least six hours before the PET/CT scans. Patients received an intravenous injection of 185 MBq (5 mCi) ^{18}F-FP-CIT and 4.1 MBq/kg of ^{18}F-FDG. ^{18}F-FP-CIT images were acquired with a 15-minute scan duration, 90 minutes after injection and ^{18}F-FDG PET images were acquired with a 15-minute scan duration, 40 minutes after injection. The spiral CT scan was performed with a 0.5 sec/rotation at 120 kVp, 200 mA, 3.75 mm slice thickness, 10.0 mm of collimation width and 9.375 mm table feed per rotation. PET images were reconstructed using the ordered subset expectation maximization algorithm (4 iterations, 32 subsets) and smoothed using a 4-mm full-width at half-maximum Gaussian filter. The final PET images had a matrix size of 256×256 with an in-plane pixel size of 0.98 mm and a slice thickness of 0.98 mm.

^{18}F-FP-CIT PET analysis

FreeSurfer software (Massachusetts General Hospital, Harvard Medical School; http://surfer.nmr.mgh.harvard.edu) was employed for processing T1-weighted brain MR images. The T1-weighted MR images underwent isovoxel reslicing to 1 mm, inhomogeneity correction, skull-stripping, and segmentation into gray and white matter. Subcortical structures were segmented and labeled utilizing a probabilistic registration technique[60] to create volume-of-interest (VOI) masks for the caudate, putamen, and cerebellum. With specific focus on the subregional analysis of the putamen, putaminal VOIs were parcellated into the following subregions: (1) anterior putamen, (2) posterior putamen, (3) posterior dorsal putamen, and (4) posterior ventral putamen. In delineating the anterior and posterior portions of the putaminal VOI, their boundary was defined as the coronal plane at the level of anterior commissure.[61] Further segmentation of the posterior putamen into dorsal and ventral components was performed using the transaxial plane defined by anterior-posterior commissure as the anatomical border.[61,62] This yielded VOI masks for the whole caudate and putamen, the anterior and posterior putamen, and the dorsal and ventral portions of the posterior putamen.

Statistical Parametric Mapping 12 (SPM12; Wellcome Trust Centre for Neuroimaging, London, UK) was utilized for processing PET images along with associated toolboxes including PETPVE12, SUIT, AAL, and HDW. All PET images were processed within the native space of each participant as determined by FreeSurfer-based segmentation of MR images. Following coregistration of individual PET images to the corresponding MR images, partial volume correction (PVC) was performed using a two-step approach: based on

subcortical segmentations, an initial PVC was performed using the Geometric Transfer Matrix (GTM) method.[63,64] Subsequently, an additional PVC step was applied using the region-based voxel-wise (RBV) method, which performs voxel-level correction based on anatomically defined structural labels.[65]

For quantitative analyses, SBR images were generated using cerebellar gray matter as the reference tissue.[66] The SBR was calculated by dividing the difference between uptake values in each voxel and the reference region by the uptake value in the reference region:

$$Specific\ binding\ ratio\ (SBR) = \frac{FPCIT\ Uptake_{TARGET} - FPCIT\ Uptake_{CEREBELLUM}}{FPCIT\ Uptake_{CEREBELLUM}}$$

Quantification of ^{18}F-FP-CIT tracer uptake in striatal subregions was obtained by overlaying the VOI template for striatal subregions onto the SBR images. Group-averaged SBR images at baseline and 12-month follow-up were generated using in-house Python code.

To visualize individual-level changes in striatal DAT binding, axial ^{18}F-FP-CIT PET images were spatially normalized to the Montreal Neurological Institute space and overlaid on a standard anatomical template. Voxel-wise percentage change maps of the SBR (Δ% SBR) were generated by calculating the relative difference in SBR values between the baseline and 12-month follow-up scans for each voxel. For visualization purposes, Δ% SBR images were thresholded at ±10%.

Immunohistochemistry

Brain sections from a 6-hydroxydopamine lesioned Sprague Dawley rat (Crl:CD(SD), Charles River Laboratories, USA) transplanted with a total of 10,000 cells in our previous preclinical dose–response study[16] were used for immunofluorescence analysis. Coronal brain sections (20 μm thickness) were blocked with 3% bovine serum albumin (BSA) in phosphate-buffered saline (PBS) containing 0.3% Triton X-100 for 1 h at room temperature, followed by incubation with primary antibodies overnight at 4 °C. Sections were then incubated with fluorescent secondary antibodies for 2 h at room temperature; fluorophore-conjugated antibody was additionally incubated for 2 h at room temperature. Nuclei were counterstained with 4′,6-diamidino-2-phenylindole (DAPI). Slides were imaged by tile scanning at 400× magnification using an LSM 980 confocal microscope (Carl Zeiss, Oberkochen, Germany).

QUANTIFICATION AND STATISTICAL ANALYSIS

Clinical outcome measures, including MDS-UPDRS part I, II, III, IV, Total, H&Y stage, NMSS, PDQ-39, SE-ADL, LEDD, PD diary (off time) and imaging outcome measure (^{18}F-FP-CIT SBR) were summarized as means (± SD) or medians (IQR). For exploratory endpoint analyses, the baseline visit (Visit 2) was used as the primary reference point. When specific assessments were not conducted at Visit 2, corresponding data from the screening visit (Visit 1) were used instead. This approach applies to all relevant endpoints, including ^{18}F-FP-CIT PET imaging.

Changes in clinical or imaging outcome measures from baseline to follow-up were compared using the Wilcoxon signed-rank test within each dose group and the Wilcoxon rank-sum test between low-dose and high-dose groups. For the imaging outcome measure, between-group comparisons were performed for the caudate (anterior and posterior) and putamen (anterior, posterior, and posterior dorsal) regions. Longitudinal changes in clinical measures (MDS-UPDRS part III OFF, NMSS, SE-ADL, PDQ-39, MMSE, MoCA, and LEDD) were analyzed using linear mixed-effects models. Models included fixed effects for time, group (low-dose and high-dose), and their interaction (time × group). For the H&Y stages, generalized linear mixed-effects models with a cumulative logit link function were used, given the ordinal nature of this outcome. Random intercepts for each patient were included to account for correlations from repeated measurements within individuals. Spearman's rank correlation coefficient was used to assess the association between the change of ^{18}F-FP-CIT SBRs in posterior dorsal putamen and MDS-UPDRS part III (OFF) scores. All analyses were performed using SAS version 9.4 (SAS Institute Inc.), with two-sided p-values < 0.05 considered statistically significant.

ADDITIONAL RESOURCES

The study is registered at ClinicalTrials.gov (NCT05887466).

Supplemental figures

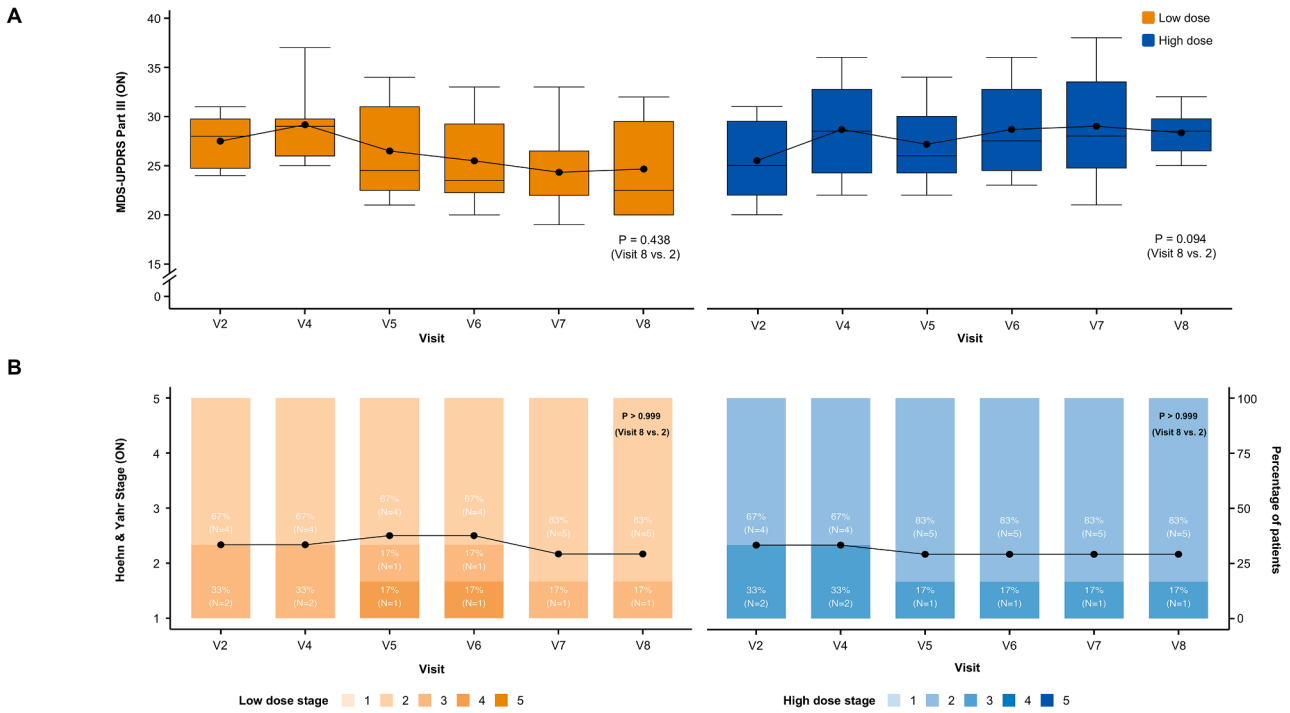

Figure S1. Longitudinal changes in clinical outcomes at on-medication state following transplantation of A9-DPC, related to Figure 3

(A) MDS-UPDRS part III scores in the on-medication state (ON). Scores for the low-dose and high-dose groups are shown at baseline and each post-transplantation visit. Scores on MDS-UPDRS part III range from 0 to 132, with higher scores indicating greater impairment on a clinician-conducted motor examination. Black dots represent mean values at each visit, and solid lines connect these means across time points. Boxplots are used to present medians (horizontal lines), IQRs (boxes), and ranges (whiskers). *p* values were calculated for comparisons between baseline and 12 months using the Wilcoxon signed-rank test. A break in the *y* axis indicates a discontinuity in scale.

(B) H&Y stages in the on-medication state. H&Y (ON) stages are shown for the low-dose and high-dose groups at baseline and each follow-up visit. H&Y stage ranges from 1 to 5, with higher stages indicating more severe motor impairment. Black dots represent mean values at each visit, and solid lines connect these means across time points. Stacked bar graphs display the distribution of patients across stages at each visit, with the percentage and number of patients indicated within each bar. *p* values were calculated for comparisons between baseline and 12 months using the Wilcoxon signed-rank test.

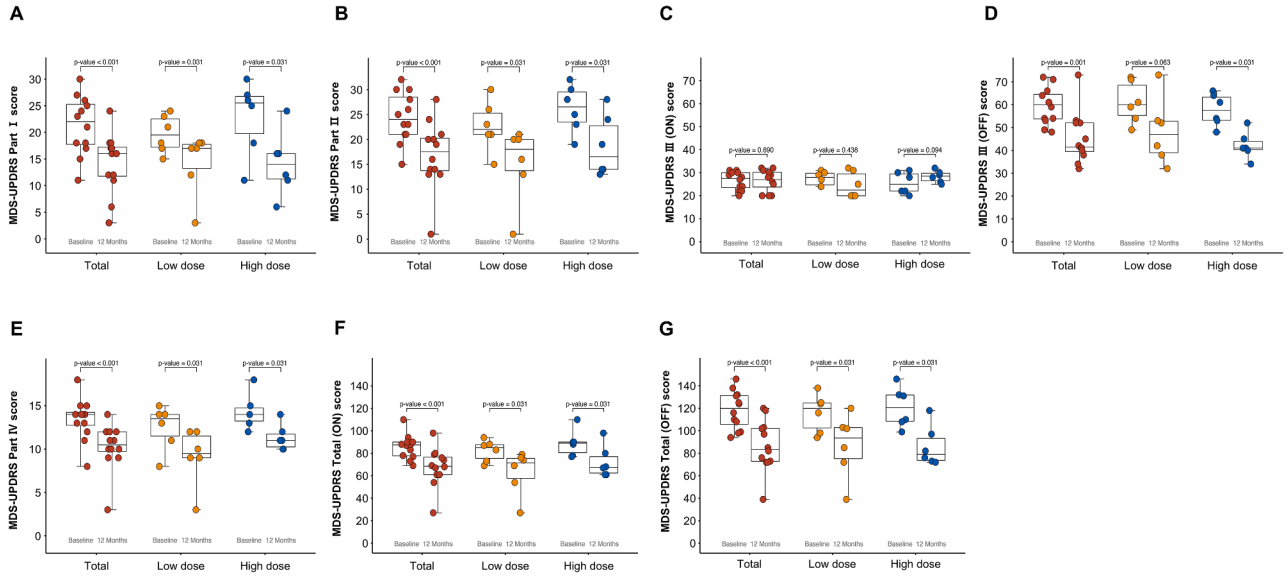

Figure S2. The MDS-UPDRS part scores at baseline and 12 months, related to Figure 3

MDS-UPDRS part I (A), part II (B), part III ON (C) and OFF (D), part IV (E), and total ON (F) and OFF (G) scores at baseline and 12 months are shown for the total cohort (n = 12), low-dose group (n = 6), and high-dose group (n = 6). Data are presented as boxplots showing the median (horizontal line), IQR (box), and range (whiskers), with individual data points overlaid. p values were calculated using the Wilcoxon signed-rank test.

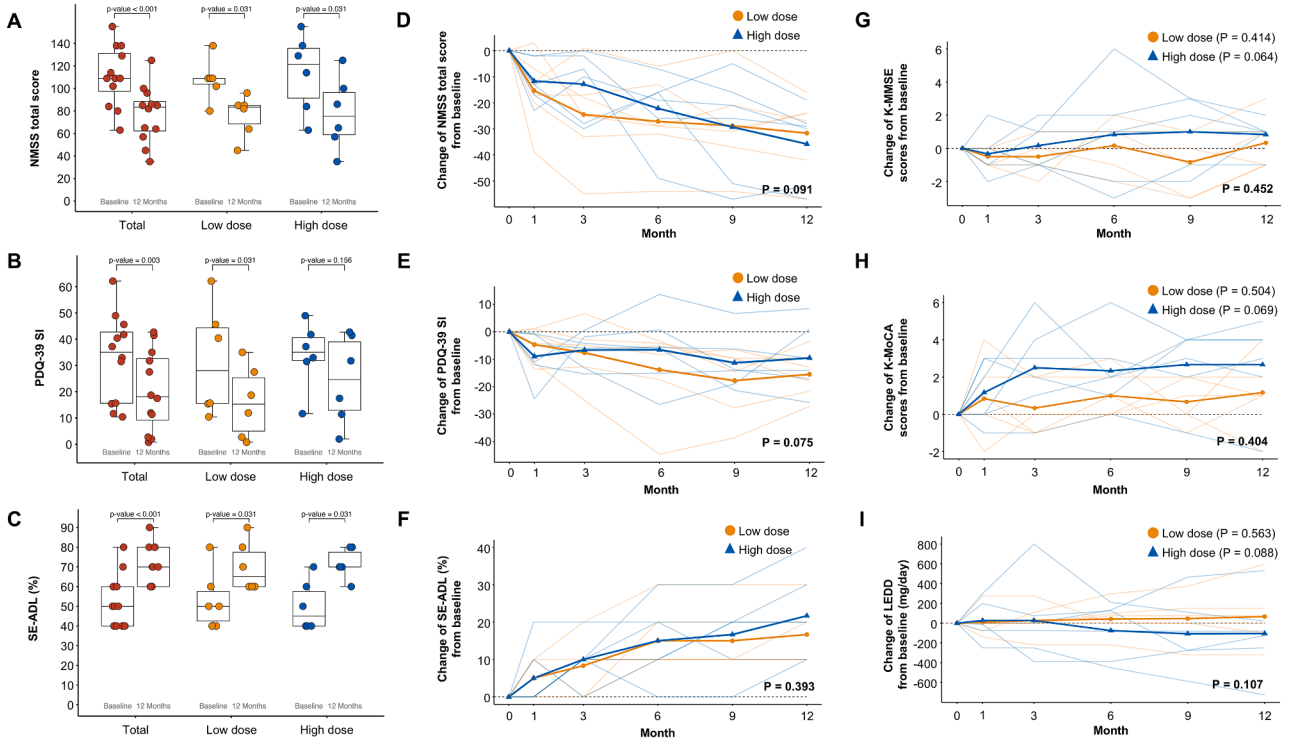

Figure S3. Longitudinal changes in NMSS, PDQ-39 SI, SE-ADL, cognitive function, and LEDD following transplantation of A9-DPC, related to Figure 3

(A–C) NMSS total score (A), PDQ-39 SI (B), and SE-ADL (C) at baseline and 12 months are shown. Data are presented as boxplots showing the median (horizontal line), IQR (box), and range (whiskers), with individual patient data points overlaid. Comparisons between baseline and 12 months were conducted using Wilcoxon signed-rank tests to assess changes over time. Lower NMSS and PDQ-39 SI scores and higher SE-ADL scores indicate improvement.

(D–F) Mean changes of the NMSS total score (D), PDQ-39 SI (E), and SE-ADL (F) from baseline to 12 months are shown. Mean trajectories are presented for the low-dose and high-dose groups, with solid lines indicating group means and thin lines indicating individual patient trajectories. *p* value indicates the statistical significance of the group × time interaction term in a linear mixed-effects model, testing whether the longitudinal trajectories differ between groups (low-dose vs. high-dose).

(G) Mean changes of the MMSE scores from baseline to 12 months are shown. Mean trajectories are presented for the low-dose and high-dose groups, with solid lines indicating group means and thin lines indicating individual patient trajectories. A linear mixed-effects model showed no significant time effect in the low-dose group ($p = 0.414$) or high-dose group ($p = 0.064$), with no significant group × time interaction ($p = 0.452$).

(H) Mean changes of the MoCA scores from baseline to 12 months are shown. Mean trajectories are presented for the low-dose and high-dose groups, with solid lines indicating group means and thin lines indicating individual patient trajectories. A linear mixed-effects model showed no significant time effect in the low-dose ($p = 0.504$) or high-dose group ($p = 0.069$), with no significant group × time interaction ($p = 0.404$).

(I) Mean changes of the LEDD from baseline to 12 months are shown. Mean trajectories are presented for the low-dose and high-dose groups, with solid lines indicating group means and thin lines indicating individual patient trajectories. A linear mixed-effects model showed no significant time effect in the low-dose ($p = 0.563$) or high-dose group ($p = 0.088$), with no significant group × time interaction ($p = 0.107$).

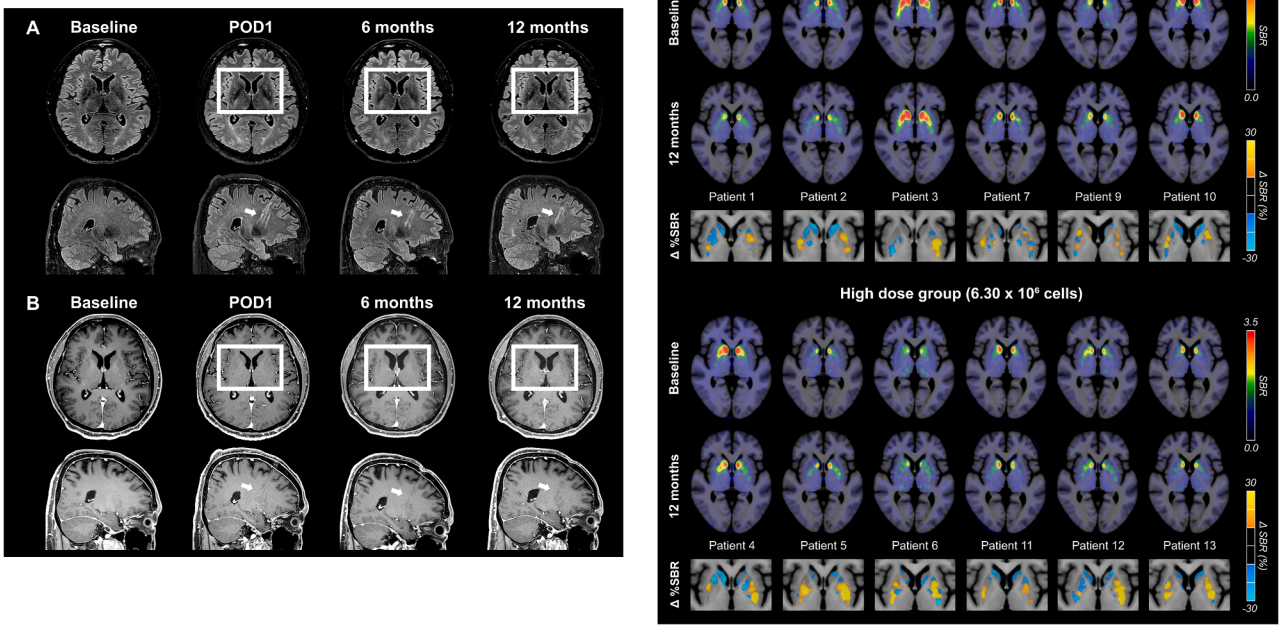

Figure S4. Representative images of brain MRI and individual-level changes in ^{18}F-FP-CIT uptake following A9-DPC transplantation, related to Figure 4

(A and B) Representative MRI scans obtained at baseline, postoperative day 1 (POD1), 6 months, and 12 months after transplantation of A9-DPC. (A) Axial and sagittal fluid-attenuated inversion recovery (FLAIR) MRI scans at each time point. (B) Axial and sagittal T1-weighted contrast-enhanced MRI scans at each time point. Evidence of cell transplantation along the needle trajectory is indicated by the white-boxed region (axial views) and arrows (sagittal views), with no evidence of hemorrhage, mass effect, or cellular overgrowth.

(C) Axial ^{18}F-FP-CIT PET scans illustrating striatal ^{18}F-FP-CIT uptake in 12 individual patients, grouped into low-dose (3.15×10^6 cells; top) and high-dose (6.30×10^6 cells; bottom) groups. For each patient, scans are shown at baseline (top row) and at 12-month follow-up (middle row). The bottom row of each panel displays voxel-wise percentage change in specific binding ratio (Δ% SBR) between baseline and follow-up. Increased DAT binding is shown in yellow, and decreased binding in blue, with changes thresholded at ±10% for visual clarity. All PET images were spatially normalized to Montreal Neurological Institute space and overlaid on a standard anatomical template.

A

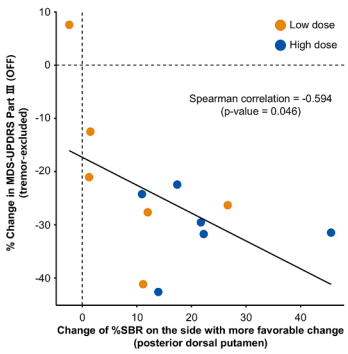

B

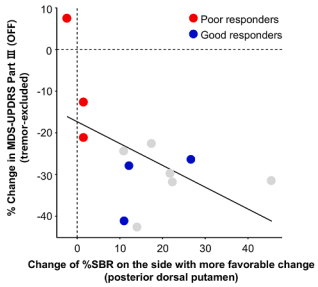

C

	Poor responders Patients (1, 7, 10) (n = 3) 3 male		Good responders Patients (2, 3, 9) (n = 3) 2 male, 1 female		Total patients of low dose group (n = 6) 5 male, 1 female	
	Median (Q1, Q3)	**Mean (SD)**	**Median (Q1, Q3)**	**Mean (SD)**	**Median (Q1, Q3)**	**Mean (SD)**
Age, yr	58.0 (53.0, 62.0)	57.7 (4.51)	61.0 (56.0, 70.0)	62.3 (7.1)	59.5 (56.0, 62.0)	60 (5.9)
Disease duration, yr	11.5 (9.0, 12.5)	11 (1.80)	9.5 (6.5, 11.5)	9.3 (2.5)	10.5 (9.0, 11.5)	10.1 (2.2)
Baseline H&Y stage (OFF)	4.0 (4.0, 4.0)	4.0 (0)	3.0 (3.0, 4.0)	3.3 (0.6)	4.0 (3.0, 4.0)	3.7 (0.5)
Baseline Part III (OFF)	71.0 (61.0, 72.0)	68.0 (6.1)	54.0 (49.0, 59.0)	54.0 (5.0)	60.0 (54.0, 71.0)	61.0 (9.1)
Baseline Part III (ON)	27.0 (24.0, 31.0)	27.3 (3.5)	29.0 (24.0, 30.0)	27.7 (3.2)	28.0 (24.0, 30.0)	27.5 (3.0)

Figure S5. Correlation between changes in ^{18}F-FP-CIT PET SBR in the posterior dorsal putamen and motor improvement, related to Figure 4

(A) Scatterplot showing the correlation between the change in ^{18}F-FP-CIT PET SBR percentage in the posterior dorsal putamen on the more favorable change side (from baseline) and the percentage change in MDS-UPDRS part III (OFF) scores, excluding the tremor subscore (n = 12). p value was calculated using Spearman's rank correlation coefficient.

(B) Scatterplot showing the correlation between the change in ^{18}F-FP-CIT PET SBR percentage in the posterior dorsal putamen on the more favorable change side (from baseline) and the percentage change in MDS-UPDRS part III (OFF) scores, excluding the tremor subscore in the low-dose group (n = 6). Patients in the low-dose group were classified as poor or good responders depending on whether both measures showed concordant and substantial improvement. Given that all patients in the high-dose group showed concordant and substantial improvement in both measures, we classified patients in the low-dose group (n = 6) into the three poor responders (patients 1, 7, and 10; marked in red) and the three good responders (patients 2, 3, and 9; marked in blue).

(C) Baseline characteristics for each group are summarized using both the median (Q1, Q3) and the mean (SD). Baseline age was comparable between the groups, whereas the good responders appeared to have less severe motor deficits at baseline, as indicated by lower MDS-UPDRS part III (OFF) score.

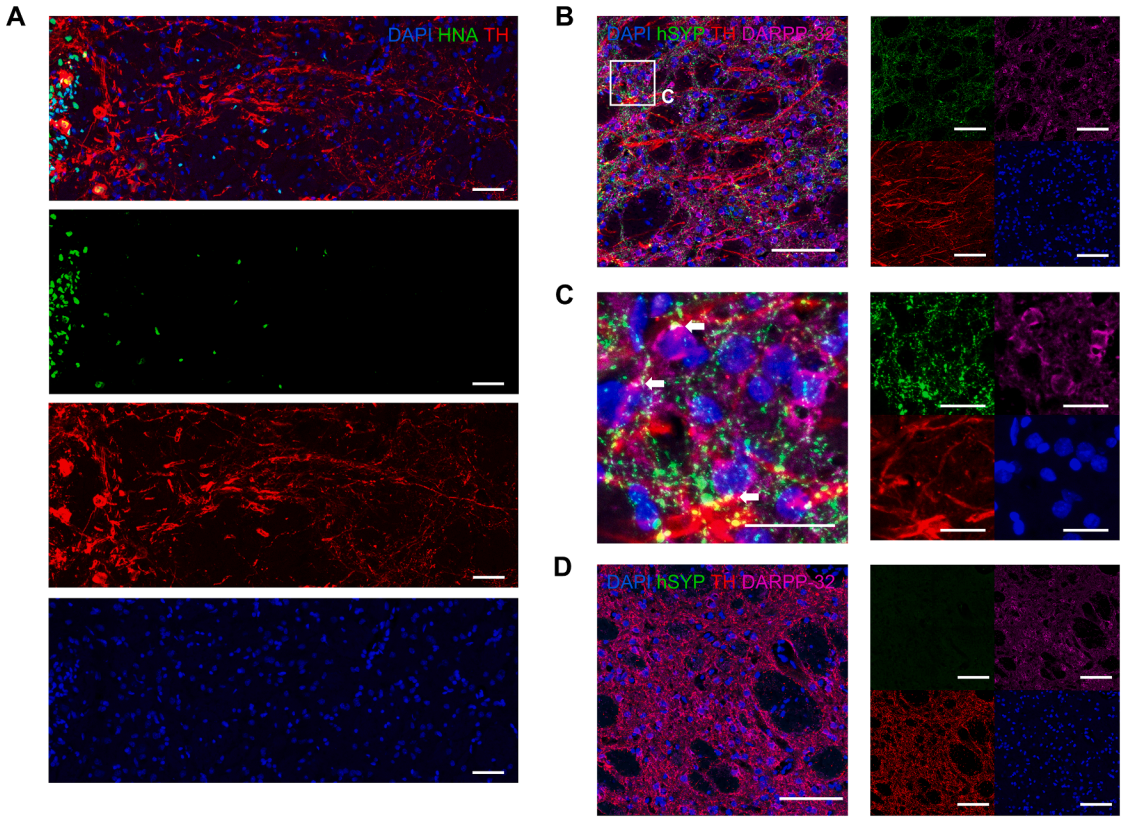

Figure S6. Representative immunohistochemical images of A9-DPC graft within the striatum of the rodent PD model, related to Figure 4

(A) Immunohistochemical image of human nuclear antigen (HNA; green), tyrosine hydroxylase (TH; red), and DAPI (blue) in the A9-DPC graft (10,000 cells) within the striatum of the 6-hydroxydopamine hydrochloride (6-OHDA) lesioned rat PD model at 24 weeks post-transplantation. TH^+ fibers of transplanted dopaminergic (DA) neurons are projecting into the host striatum. Scale bar, 50 μm.

(B) Immunohistochemical image of human synaptophysin (hSYP; green), TH (red), cAMP-regulated phosphoprotein of 32 kDa (DARPP-32; magenta), and DAPI (blue) in the ipsilateral striatum of A9-DPC graft with TH^+ fibers. Scale bar, 100 μm.

(C) High-magnification image of the white-boxed region in (B). The arrows indicate hSYP signals at the interface between TH^+ fiber and DARPP-32^+ host medium spiny neurons. Scale bar, 25 μm.

(D) Immunohistochemical image of hSYP (green), TH (red), DARPP-32 (magenta), and DAPI (blue) in the contralateral striatum of the A9-DPC graft. Scale bar, 100 μm.

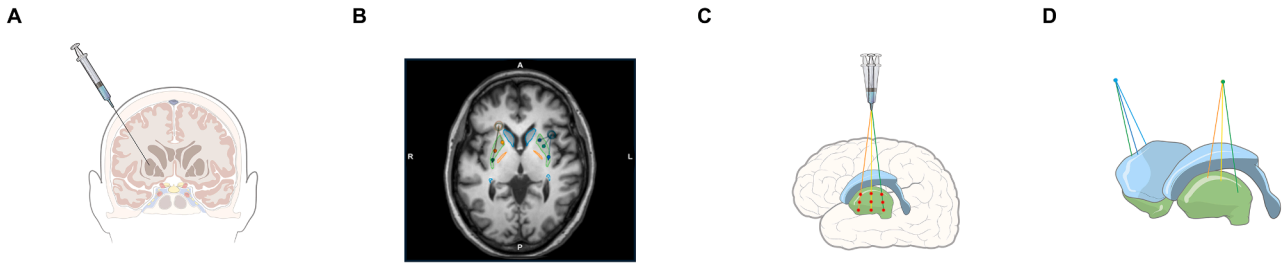

Figure S7. Overview of stereotactic transplantation procedures, related to STAR Methods

(A) Schematic of stereotactic injection targeting the bilateral putamen.

(B) MRI-based trajectory planning using stereotactic planning software and the Leksell stereotactic frame G.

(C) Schematic depiction of three planned trajectories (anterior, middle, and posterior) per hemisphere, each with three injection sites, resulting in 18 deposits per subject.

(D) Three-dimensional illustration of bilateral putamen (green) injection trajectories.